

The following contains the comments of the referee (black), our replies (blue) indicating changes that will be made to the revised document (red).

### **Reviewer #1**

This is an excellent and very careful study of the kinetics of the reaction of OH radical with NO<sub>2</sub>, a reaction of central atmospheric significance. The main finding associated with this work (the second paper from this group on this reaction) is the finding of a significant enhancement to the OH/NO<sub>2</sub> rate coefficient in the presence of water vapor. This enhancement is quantified in both N<sub>2</sub> and He bath gas, and as a function of temperature. The data appear to be of the highest quality, previous data are discussed in detail, and the modeling work adds significantly to the atmospheric context, and hence the overall value of the manuscript. Overall a superb study! I recommend publication in ACP, after consideration of the minor comments listed below.

We thank the reviewer for the careful review and the positive assessment of our manuscript.

L12 – molecule misspelled. Corrected

L64 – exponent should be +3. Corrected

L127 – evaluation of atmospheric. Corrected

L148- Maybe it is obvious, but it could be added to the text that fitting with an increased  $F_c$  gives a lower  $k_0$ , (which doesn't fit the data).

We have added:

We note that using a higher  $F_c=0.39$  resulted in a lower value of  $k_0^{\text{He}}$  equal to  $1.0 \times 10^{-30} \text{ cm}^6 \text{ molecule}^{-2} \text{ s}^{-1}$ .

Page 4,5 - The pure He data are taken here at 292 K, somewhat below other 'room temperature' datasets that comparisons are being made with. Has this been taken into account? If not, could this account for at least some of the systematic discrepancies with D'Ottone or Morley?

In Figure 1, we did not attempt to apply any corrections to previous works to account for temperature differences. In the more rigorous comparison of our work with others (Fig S3-S5), we used our parametrization at the given temperatures of the previous studies.

We now write in the Figure S3, S4 and S5 captions the temperature for which  $k(T,p)$  was calculated.

On a related point, there is a T-dependence to the He  $k_0$  that appears in various places (captions to Fig 2, Fig 4b, L252). What is the origin of this value? (I think it is mostly unnecessary).

The T-dependence in He was determined in our laboratory over a small range of temperatures (277, 292 and 332 K) and pressures. We have added the data points used to determine  $m(\text{He})$  in Table 1, a Figure (S10) in the supplementary information and the text below:

The T-dependence factor in He,  $m(\text{He})$ , was determined to be 3.1 over the temperature range from 277 to 332 K (Table 1 and Figure S6).

$T$ (K)	$p$ (Torr)	$M^a$	OH precursor	$k_1^b$
277	48.6	1.68	H <sub>2</sub> O <sub>2</sub>	$1.59 \pm 0.14$
292	25.1	0.83	H <sub>2</sub> O <sub>2</sub> <sup>c</sup>	$0.75 \pm 0.07$
	50.0	1.65	H <sub>2</sub> O <sub>2</sub>	$1.37 \pm 0.08$
	75.1	2.47	H <sub>2</sub> O <sub>2</sub>	$1.88 \pm 0.12$
	102.9	3.39	HNO <sub>3</sub>	$2.32 \pm 0.15$
	206.9	6.81	HNO <sub>3</sub> <sup>d</sup>	$3.73 \pm 0.25$
	300.7	9.89	HNO <sub>3</sub>	$4.64 \pm 0.29$
	405.8	13.35	HNO <sub>3</sub>	$5.54 \pm 0.37$
	495.6	16.30	HNO <sub>3</sub>	$6.29 \pm 0.40$
	595.0	19.57	HNO <sub>3</sub>	$6.83 \pm 0.42$
	689.1	22.67	HNO <sub>3</sub>	$7.46 \pm 0.46$
332	28.1	0.82	H <sub>2</sub> O <sub>2</sub>	$0.60 \pm 0.06$
	56.8	1.65	H <sub>2</sub> O <sub>2</sub>	$0.99 \pm 0.08$
	85.4	2.48	H <sub>2</sub> O <sub>2</sub>	$1.34 \pm 0.10$

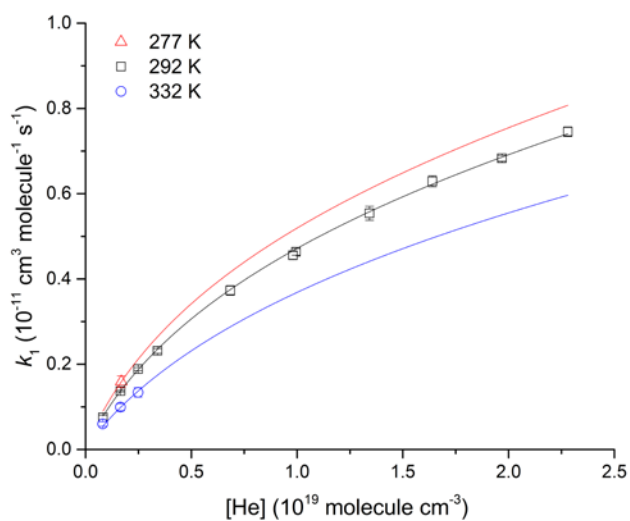


Figure S6. Values of  $k_1$  as a function of He concentration at 277, 292 and 332 K. Errors are  $2\sigma$  statistical only. The solid line is a fit to our data using Eqn. (4) with  $k_0 = 1.4 \times 10^{-30} \text{ cm}^6 \text{ molecule}^{-2} \text{ s}^{-1}$ ,  $k_\infty = 6.3 \times 10^{-11} \text{ cm}^3 \text{ molecule}^{-1} \text{ s}^{-1}$ ,  $F_c = 0.32$ ,  $m = 3.1$  and  $n = 0$ .

L209- delete molecules **Corrected**

L252 – temperature dependence **Corrected**

L254 – delete use **Corrected**

L275 and forward – The tests for HONO and HNO<sub>3</sub> are really nice !

L297 – temperature instead of temperatures **Corrected**

L342 – H<sub>2</sub>O, not HO<sub>2</sub>, as product of (R7) **Corrected**

L406 – short at **Corrected**

L408 – temperature and pressure conditions **Corrected**

The following contains the comments of the referee (black), our replies (blue) indicating changes that will be made to the revised document (red).

## **Reviewer #2**

The manuscript describes the determination of the rate constant of the OH + NO<sub>2</sub> reaction with He and N<sub>2</sub> as bath gases in presence and absence of gaseous H<sub>2</sub>O. A quasi-static reaction cell was used, and OH was produced by pulsed laser photolysis of HNO<sub>3</sub>, H<sub>2</sub>O<sub>2</sub>, or O<sub>3</sub>/H<sub>2</sub>O mixtures. Pseudo-first order conditions with respect to [OH] were applied. The OH concentration was monitored time-resolved by laser-induced fluorescence, and the (crucial) NO<sub>2</sub> concentration was carefully determined with two different absorption-spectroscopic approaches. A notable increase of the OH + NO<sub>2</sub> rate constant in He and N<sub>2</sub> when H<sub>2</sub>O is present was observed and associated with a particularly high efficiency of H<sub>2</sub>O for collisional stabilization of the HNO<sub>3</sub> product. Non-linear mixing rules for the collisional efficiencies seem to apply. Very careful parameterizations and statistical evaluations of the experimental results, including earlier literature data, were performed and discussed in great detail, also with respect to branching between HONO<sub>2</sub> and HOONO as reaction products. The newly parameterized rate constant is incorporated in a 3D chemical transport model, and effects on quantities such as the atmospheric HNO<sub>3</sub>/NO<sub>2</sub> ratio, the atmospheric concentration of OH, or the HOONO/HO<sub>2</sub>NO<sub>2</sub> ratio are assessed. All in all, this is a very nice paper bridging high-level state-of-the-art laboratory measurements with global atmospheric modeling. So the topic is at the very heart of ACP, and I recommend publication essentially 'as is' with only very few, very minor points to be considered by the authors:

We thank the reviewer for the careful review and the positive assessment of our manuscript.

line 35: 'gases' should probably read 'gas' **Corrected**

line 68: 'O<sub>3</sub>-H<sub>2</sub>O' should probably better read 'O<sub>3</sub>/H<sub>2</sub>O' **Corrected**

Tables 1 and 2: please specify/explain M

In Table 1, we modified the caption below with:

**Molecular density M(He) in units of 10<sup>18</sup> molecule cm<sup>-3</sup>**

In Table 2, we modified in the caption,

**Molecular density M(He-H<sub>2</sub>O) or M(N<sub>2</sub>-H<sub>2</sub>O) in units of 10<sup>18</sup> molecule cm<sup>-3</sup>**

Fig. 1, figure caption: please give the parameters m and n

The figure 1 caption now reads:

**The solid line is a fit to our data using Eqn. (4) with  $k_0 = 1.4 \times 10^{-30} \text{ cm}^6 \text{ molecule}^{-2} \text{ s}^{-1}$ ,  $k_\infty = 6.3 \times 10^{-11} \text{ cm}^3 \text{ molecule}^{-1} \text{ s}^{-1}$ ,  $F_c = 0.32$ ,  $m=3.1$  and  $n=0$ .**

Fig. 2, figure caption: please give the parameter n

The figure 2 caption now reads:

**The black line is our parameterisation with  $k_0 = 1.4 \times 10^{-30} \text{ cm}^6 \text{ molecule}^{-2} \text{ s}^{-1}$ ,  $k_\infty = 6.3 \times 10^{-11} \text{ cm}^3 \text{ molecule}^{-1} \text{ s}^{-1}$ ,  $m = 3.1$ ,  $n=0$  and  $F_c = 0.32$ .**

The following contains the comments of the referee (black), our replies (blue) indicating changes that will be made to the revised document (red).

### **Reviewer #3**

This manuscript presents the first study of the effectiveness of H<sub>2</sub>O as a third body on the recombination of OH with NO<sub>2</sub>. This careful experimental study shows that water vapor is much more effective than N<sub>2</sub> or O<sub>2</sub> in causing recombination. It also presents a global modeling study of a new parameterization of the OH + NO<sub>2</sub> reaction as compared to the IUPAC and JPL recommendations; this parameterization uses the results of a previous study showing that O<sub>2</sub> and N<sub>2</sub> have different efficiencies in quenching the products of OH + NO<sub>2</sub>. The modeling suggests that HOONO could be a non-negligible reservoir of NO<sub>x</sub> in some parts of the atmosphere. This is a very important paper that is clearly in the scope of ACP. There are no major problems with the manuscript, but a few of points should be clarification or emphasized more strongly before publication in ACP.

We thank the reviewer for the careful review and the positive assessment of our manuscript.

My major concern about this manuscript is actually rather minor: In the global modeling, it is not clear how much of the affects of the new parameterization, occurs due to water vapor and how much due to the use of the results of the author's previous paper on N<sub>2</sub> vs O<sub>2</sub> as colliders. This should be made clear.

As we already mention, the impact of H<sub>2</sub>O is limited to the boundary-layer (Fig. 5), above which the H<sub>2</sub>O concentration decreases rapidly. We now emphasise this by writing:

The presence of water vapour does not impact on values of  $k_1$  above the boundary layer.

The enhancement of the quenching of the energized HNO<sub>3</sub> intermediate (HNO<sub>3</sub> \*) due to H<sub>2</sub>O vapor is presumably due to the strong hydrogen bonding between the two (stronger than OH-H<sub>2</sub>O or NO<sub>2</sub>-H<sub>2</sub>O). It would be good to make this explicit and add some references to the literature on the HONO<sub>2</sub>-HOH complex.

We have added text mentioning the HNO<sub>3</sub> – H<sub>2</sub>O complex:

Water vapour is therefore a factor  $\approx 8$  more efficient than O<sub>2</sub>, and a factor  $\sim 6$  more efficient than N<sub>2</sub> as a quencher of the HO-NO<sub>2</sub> intermediate, which is qualitatively consistent with known strong binding (40 kJ mol<sup>-1</sup>) in the HNO<sub>3</sub>-H<sub>2</sub>O complex (Tao et al., 1996).

There must be previous field work measuring [NO<sub>2</sub>]/[HONO<sub>2</sub>] and corresponding modeling work that did or did not find discrepancies. It seems that the authors should refer discuss a few of these, at least briefly.

This is an old problem in atmospheric chemistry. HNO<sub>3</sub> is not formed solely in the reaction between OH and NO<sub>2</sub> but also in heterogeneous processes that hydrolyse N<sub>2</sub>O<sub>5</sub>, the rate of which depends on poorly constrained factors such as e.g. the aerosol surface area. Uncertainties in modelled OH are large as are uncertainties for HNO<sub>3</sub> measurements, which in the boundary layer reflect deposition to surfaces, again poorly constrained. In short, uncertainties in kinetic parameters are only one factor that influence NO<sub>2</sub> and HNO<sub>3</sub> ratios and this issue is too complex to deal with properly in this manuscript.

Minor Issues:

Line 12: “molecule” is missing an “l” **Corrected**

Line 45: “being” should be “is” **Corrected**

Line 50-52. The sentence beginning “Theoretical calculations...” might better appear immediately after the discussion of the chaperone mechanism, rather than after the introduction of enhanced collider gases.

**Corrected as suggested**

line 68 “prevented” should be “preventing” **Corrected**

line 75: “in Tables 1 and 2.” might better be phrased as “in the notes to Tables 1 and 2.”

**Corrected as suggested**

It might help orient readers if the manuscript provided some idea of the conditions under which the  $\text{OH} + \text{NO}_2 \rightarrow \text{HONO}_2$  is nearly in the low-pressure limit and high-pressure limit.

**We added the following text**

**Under the conditions of  $T$  and  $p$  relevant for atmospheric chemistry, the title reaction is in the fall-off regime.**

Line 102: The manuscript states that the low vapor pressure of water prevents it from being used as a bath gas by itself, but 5 Torr of water vapor is roughly equivalent of 50 Torr of He. So I think that it would be clearer to say that it is not possible to determine  $k_0(\text{H}_2\text{O})$  by using pure water vapor as a bath gas.

**This is correct. We prefer to remove this statement completely.**

Lines 205 ff. “In other words....” It is not clear to this reader how it follows from the previous text that the total rate constant of a  $\text{H}_2\text{O}-\text{N}_2$  bath gas is not the sum of individual rate constants  $k(\text{P}_i, T)$ , where  $i = \text{H}_2\text{O}$  or  $\text{N}_2$ . It seems like a step of the logic has not been made explicit, and that it would help the reader if the manuscript made the logic clearer.

**Starting the sentence with “In other words” was indeed confusing.**

**We have removed this.**

In Section 3.2.1, it would be helpful to indicate the pressures at which  $k(\text{P}, 300)$  deviates by more than 10% from the low-pressure and high-pressure limits. This would help orient the reader.

**It is not obvious what insight this brings as there is no physical meaning associated with a 10% deviation. We believe this would be confusing and prefer not to follow this suggestion.**

Line 298: the pressures only add up to 990 mbar, not 1 bar.

**We now write:**

**The pressure of water vapour is 34 mbar, those of  $\text{O}_2$  and  $\text{N}_2$  are then 210 and 756 mbar, respectively**

Lines 334 ff. If I understand correctly, the manuscript takes the branching ratio between reactions (1a) and (1b) from previous work. This is equivalent to assuming that water vapor

enhances both rate constants to the same extent. This assumption should be made very explicit in the manuscript.

We have added the following sentence to make this clear.

We assume  $\alpha$  is independent of water vapour.

Lines 432-433: Are the H-OONO and H-OONO<sub>2</sub> bond energies known from computational chemistry (well enough to determine which is stronger)?

We are not aware of such calculations and are not in a position to do them ourselves. The text simply introduces the possibility that the OH rate coefficients for H-OONO and H-OONO<sub>2</sub> are different and suggests that theoretical calculations would be useful. Hopefully, someone will conduct such calculations and calculate the relative rate coefficient.

Figure 3 lacks error bars.

The error bars are already on the plot but are in most case smaller than the symbol. We have added to the caption:

With a few exceptions, the error bars ( $2\sigma$ ) are generally smaller than the symbols.

Table 2: The caption lists the range of [HOOH] used for the He-H<sub>2</sub>O experiments twice. I suspect one of these is for the N<sub>2</sub>-H<sub>2</sub>O experiments. Correction made.

# Kinetics of the OH + NO<sub>2</sub> reaction: Effect of water vapour and new parameterisation for global modelling.

Damien Amedro<sup>1</sup>, Matias Berasategui<sup>1</sup>, Arne J. C. Bunkan<sup>1</sup>, Andrea Pozzer<sup>1</sup>, Jos Lelieveld<sup>1</sup> and John N. Crowley<sup>1</sup>

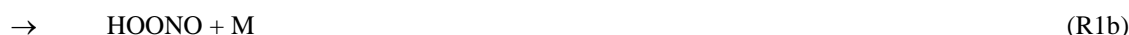
<sup>1</sup>Division of Atmospheric Chemistry, Max-Planck-Institute for Chemistry, 55128 Mainz, Germany

Correspondence to: John N. Crowley (john.crowley@mpic.de)

**Abstract.** The effect of water vapour on the rate coefficient for the atmospherically important, termolecular reaction between OH and NO<sub>2</sub> was determined in He-H<sub>2</sub>O (277, 291 and 332 K) and N<sub>2</sub>-H<sub>2</sub>O bath gases (292 K). Combining pulsed laser photolytic generation of OH and its detection by laser induced fluorescence (PLP-LIF) with in-situ, optical measurement of both NO<sub>2</sub> and H<sub>2</sub>O we were able to show that (in contrast to previous investigations) the presence of H<sub>2</sub>O increases the rate coefficient significantly. We derive a rate coefficient for H<sub>2</sub>O bath gas at the low-pressure limit ( $k_0^{\text{H}_2\text{O}}$ ) of  $15.9 \times 10^{-30} \text{ cm}^6 \text{ molecule}^{-2} \text{ s}^{-1}$ . This indicates that H<sub>2</sub>O is a more efficient collisional quencher (by a factor of  $\approx 6$ ) of the initially formed HO-NO<sub>2</sub> association complex than N<sub>2</sub> and a factor  $\approx 8$  more efficient than O<sub>2</sub>. Ignoring the effect of water-vapour will lead to an underestimation of the rate coefficient by up to 15% e.g. in the tropical boundary layer. Combining the new experimental results from this study with those from the companion paper in which we report rate coefficients obtained in N<sub>2</sub> and O<sub>2</sub> bath gases (Amedro et al., 2019) we derive a new parameterisation for atmospheric modelling of the OH + NO<sub>2</sub> reaction and use this in a chemical transport model (EMAC) to examine the impact of the new data on the global distribution of NO<sub>2</sub>, HNO<sub>3</sub> and OH. Use of the new parameters (rather than those given in the IUPAC and NASA evaluations) result in significant changes in the HNO<sub>3</sub> / NO<sub>2</sub> ratio and NO<sub>x</sub> concentrations, the sign of which depends on which evaluation is used as reference. The model predicts the presence of HOONO (formed along with HNO<sub>3</sub> in the title reaction) in concentrations similar to those of HO<sub>2</sub>NO<sub>2</sub> at the tropical tropopause.

## 1 Introduction

In our recent study of the title reaction (Amedro et al., 2019), we reported extensive measurements of the rate constant ( $k_1$ ) for the termolecular reaction between OH and NO<sub>2</sub> (R1) in N<sub>2</sub> and O<sub>2</sub> bath gas over a large range of temperature and pressures.



Reaction (R1) converts NO<sub>2</sub> to nitric acid (HNO<sub>3</sub>) and peroxyxynitrous acid (HOONO), and its rate strongly influences the relative abundance of atmospheric NO<sub>x</sub> (NO<sub>2</sub> + NO) and longer-lived “reservoirs” of NO<sub>x</sub> which include e.g. HNO<sub>3</sub> and organic nitrates. It also converts OH (the main initiator of atmospheric oxidation) to a long-lived reservoir, HNO<sub>3</sub>. As the abundance of OH and NO<sub>x</sub> directly impact on photochemical ozone formation and the lifetimes of greenhouse gases, reaction (R1) may be considered one of the most important gas-phase processes in atmospheric science (Newsome and Evans, 2017). As outlined by Amedro et al. (2019), the rate coefficients and product-branching for this reaction are dependent on pressure and temperature and also on the bath-gas identity, i.e. the identity of the collision partner, M in reaction (R1). The per collision efficiency of energy transfer from the initially “hot” association complex to bath gas can vary considerably, with more complex bath gases possessing more degrees of freedom and bonds with similar vibrational frequencies to those in the association complex being generally more efficient. In this sense, we may expect H<sub>2</sub>O to be better than N<sub>2</sub> or O<sub>2</sub> in quenching [HO-NO<sub>2</sub>]<sup>#</sup>. In this second part of our study of the reaction between OH and NO<sub>2</sub>, we extend the experiments to H<sub>2</sub>O and He bath-gases. After N<sub>2</sub> ( $\approx 78\%$ ) and O<sub>2</sub> ( $\approx 21\%$ ) water vapour is the third most abundant gaseous species in the lower atmosphere. Its



concentration is highly variable in time and space, varying in mixing ratio from a few percent at sea level to parts-per-million in the stratosphere. Most of the atmosphere's water vapour is present in the planetary boundary layer where its average mixing ratio on the global scale is  $\approx 1\%$  but which may exceed 5% in tropical regions.

The effect of water vapour on gas-phase radical-reactions has been the subject of numerous studies (Buszek et al., 2011) and is sometimes interpreted in terms of formation of  $\text{H}_2\text{O}$ -radical complexes leading, via a chaperone type mechanism, to an increase in the rate constant. An important example of this is the  $\text{HO}_2$  self-reaction for which the rate constant increases by a factor of up to two in the presence of water vapour due to formation of an  $\text{HO}_2\text{-H}_2\text{O}$  complex (Lii et al., 1981; Kircher and Sander, 1984). Theoretical calculations (Allodi et al., 2006; Sadanaga et al., 2006; Thomsen et al., 2012) suggest that, under our experimental conditions, the fraction of OH and  $\text{NO}_2$  clustered with  $\text{H}_2\text{O}$  is  $< 0.1\%$  which is insufficient to significantly impact on  $k_1$ .

On the other hand, the role of  $\text{H}_2\text{O}$  as a collision partner in termolecular, atmospheric reactions has rarely been reported though its potential impact has been highlighted (Troe, 2003). Indeed, water vapour is known to be a more efficient third-body collider, by up to an order of magnitude compared to  $\text{N}_2$  in termolecular reactions such as  $\text{H} + \text{H} + \text{M}$ ,  $\text{H} + \text{OH} + \text{M}$  and  $\text{H} + \text{O}_2 + \text{M}$  (Getzinger and Blair, 1969; Michael et al., 2002; Fernandes et al., 2008; Shao et al., 2019).

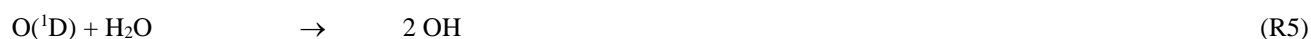
The conclusions of three previous experiments examining the role of  $\text{H}_2\text{O}$  in kinetic studies of reaction (R1) are highly divergent, with the addition of  $\text{H}_2\text{O}$  found to 1) increase the rate coefficient (Simonaitis and Heicklen, 1972), 2) have no measureable effect (D'Ottone et al., 2001) or 3) even reduce it (Sadanaga et al., 2006). The overall aim of this research was to clarify these differences and provide quantitative data on the third-body efficiency of  $\text{H}_2\text{O}$  for the title reaction. Based on the kinetic data for the water vapour effect reported in this manuscript and in  $\text{N}_2$  and  $\text{O}_2$  presented in the first part of this study (Amedro et al., 2019) we have generated a new parameterisation for the overall rate coefficient,  $k_1$ , and examined its impact on atmospheric OH,  $\text{NO}_x$  and  $\text{NO}_y$  in a global chemical transport model.

## 2. Experimental details

The details of the experimental set-up have been published previously (Wollenhaupt et al., 2000; Amedro et al., 2019) and only a brief description is given here.

### 2.1 PLP-LIF technique

The experiments were carried out in a quartz reactor of volume  $500\text{ cm}^3$  which was thermostatted to the desired temperature by circulating a 60:40 mixture of ethylene glycol-water. The pressure in the reactor was monitored with 100 and 1000 Torr capacitance manometers. Flow rates were chosen so that a fresh gas sample was available for photolysis at each laser pulse (laser frequency, 10 Hz), thus preventing build-up of products. Pulses of 248 nm laser light ( $\approx 20\text{ ns}$ ) for OH generation from  $\text{HNO}_3$ ,  $\text{H}_2\text{O}_2$  and  $\text{O}_3/\text{H}_2\text{O}$  precursors were provided by an excimer laser (Compex 205 F, Coherent) operated using KrF.



OH concentrations ( $10^{11} - 10^{12}\text{ molecule cm}^{-3}$ ) were similar to those reported by Amedro et al. (2019) and the same arguments, which rule out significant influence of secondary reactions, apply. The concentration ranges of the  $\text{H}_2\text{O}_2$ ,  $\text{HNO}_3$  and  $\text{O}_3$  precursors are listed in the notes to Tables 1 and 2.

OH was detected following excitation of the OH  $A^2\Sigma(v'=1) \leftarrow X^2\Pi(v''=0)$  transition (Q11(1) at 281.997 nm using a YAG-pumped dye laser (Quantel-Brilliant B and Lambda-Physik Scanmate). OH fluorescence was detected by a photomultiplier tube (PMT) screened by a 309 nm interference filter and a BG 26 glass cut-off filter.

## 2.2 On-line absorption measurement of NO<sub>2</sub> and H<sub>2</sub>O concentration

As discussed by Amedro et al. (2019), the determination of the NO<sub>2</sub> concentration is critical for accurate measurement of  $k_1$ . We therefore deployed in-situ, broad-band (405 – 440 nm) and single wavelength (365 nm) optical absorption spectroscopy. The former was located prior (in flow) to the quartz-reactor, the latter was located behind the quartz-reactor. Using the broadband cell, the NO<sub>2</sub> concentration was retrieved by least square fitting from 405 to 440 nm to a reference spectrum (Vandaele et al., 2002) degraded to the resolution of our spectrometer. Simultaneously, we measured NO<sub>2</sub> at 365 nm using the absorption cross-section  $5.89 \times 10^{-19} \text{ cm}^2 \text{ molecule}^{-1}$  determined previously by Amedro et al. (2019) who give a detailed description of the NO<sub>2</sub> concentration measurements and the choice of reference spectrum. For the temperatures used in this study, corrections to the NO<sub>2</sub> concentration due to formation of the N<sub>2</sub>O<sub>4</sub> dimer were not necessary. For the present experiments, a third absorption cell ( $l = 40 \text{ cm}$ ) was placed downstream of the quartz-reactor to measure the H<sub>2</sub>O concentration at 184.95 nm. This set-up used a low-pressure Hg-Penray lamp isolated with a 185 nm interference filter as light source. Optical extinction was converted to concentrations using a cross-section of  $7.14 \times 10^{-20} \text{ cm}^2 \text{ molecule}^{-1}$  (Cantrell et al., 1997).

## 2.3 Chemicals

N<sub>2</sub> and He (Westfalen 99.999%) were used without further purification. H<sub>2</sub>O<sub>2</sub> (AppliChem, 50 wt. %) was concentrated to >90 wt.% by vacuum distillation. Anhydrous nitric acid was prepared by mixing KNO<sub>3</sub> (Sigma Aldrich, 99%) and H<sub>2</sub>SO<sub>4</sub> (Roth, 98%), and condensing HNO<sub>3</sub> vapour into a liquid nitrogen trap. NO (3.5 AirLiquide) was purified of other nitrogen oxides by fractional, vacuum distillation and then converted to NO<sub>2</sub> via reaction with a large excess of O<sub>2</sub>. The NO<sub>2</sub> thus made was trapped in liquid N<sub>2</sub> and the excess O<sub>2</sub> was pumped out. The resulting NO<sub>2</sub> was stored as a mixture of ~0.5% NO<sub>2</sub> in N<sub>2</sub> or ~5.5% NO<sub>2</sub> in He. Distilled H<sub>2</sub>O (Merck, Liquid Chromatography grade) was degassed before use and kept at constant temperature.

## 3 Results and Discussion

### 3.1 Measurements of $k_1$ in He bath-gas and comparison with literature

Our study of the role of H<sub>2</sub>O as collision partner in reaction (R1) was carried out in mixtures of He-H<sub>2</sub>O and N<sub>2</sub>-H<sub>2</sub>O. In order to separate the effects of H<sub>2</sub>O and He, we also required accurate rate coefficients for pure He bath gas, which we describe below. As for the N<sub>2</sub> and O<sub>2</sub> bath-gas datasets (Amedro et al., 2019), the experiments were carried out under pseudo-first-order conditions ( $[\text{NO}_2] \gg [\text{OH}]$ ) so that Eqn. 1-2 describe the decay of OH and the derivation of the bimolecular rate coefficient,  $k_1$ .

$$[\text{OH}]_t = [\text{OH}]_0 \exp(-k't) \quad (1)$$

where  $[\text{OH}]_t$  is the concentration ( $\text{molecule cm}^{-3}$ ) at time  $t$  after the laser pulse.  $k'$  is the pseudo-first order rate coefficient and is defined as

$$k' = k_1[\text{NO}_2] + k_d \quad (2)$$

where  $k_d$  ( $\text{s}^{-1}$ ) accounts for OH-loss due to diffusion out of the reaction zone and reaction with its photolytic precursors such as HNO<sub>3</sub> or H<sub>2</sub>O<sub>2</sub>.

An exemplary dataset illustrating OH decays and a plot of  $k'$  versus  $[\text{NO}_2]$  is given in Fig. S1 of the supplementary information).

115 Values of  $k_1$  obtained in He bath-gas (25-690 Torr, 292 K) are summarised in Fig. 1 and 2 and listed in Table 1. The kinetics of termolecular reactions can be described by the Lindemann-Hinshelwood mechanism whereby the rate constant at the low-pressure limit ( $k_0$ , units in  $\text{cm}^6 \text{ molecule}^{-2} \text{ s}^{-1}$ ) is proportional to the pressure and at the high pressure limit ( $k_\infty$ , units in  $\text{cm}^3 \text{ molecule}^{-1} \text{ s}^{-1}$ ) is independent of pressure. In the intermediate pressure range, the fall-off regime, the rate coefficient is a function of both low-pressure ( $k_0$ ) and high-pressure ( $k_\infty$ ) rate coefficients and the (reaction-partner dependent) broadening factor  $F$  which accounts for the lower rate constant measured in the fall-off regime than predicted by the Lindemann-Hinshelwood mechanism reactions (Troe, 1983). Under the conditions of  $T$  and  $p$  relevant for atmospheric chemistry, the title reaction is in the fall-off regime.

$$k = \frac{k_0[M]k_\infty}{k_0[M] + k_\infty} F \quad (3)$$

125

The solid lines in Figs. 1 and 2 are fits according to the Troe formalism for termolecular reactions (Troe, 1983) as adopted by the IUPAC panel in their evaluation of atmospheric reactions:

$$k(P, T) = \frac{k_0 \left(\frac{T}{300}\right)^{-m} [M] k_\infty \left(\frac{T}{300}\right)^{-n}}{k_0 \left(\frac{T}{300}\right)^{-m} [M] + k_\infty \left(\frac{T}{300}\right)^{-n}} F \quad (4)$$

130 where  $T$  is the temperature in Kelvin,  $[M]$  is the bath-gas concentration in molecule  $\text{cm}^{-3}$ ,  $m$  and  $n$  are dimensionless temperature exponents.

The broadening factor,  $F$ , is:

$$\log F = \frac{\log F_c}{1 + \left[ \log \left( \frac{k_0 \left(\frac{T}{300}\right)^{-m} [M]}{k_\infty \left(\frac{T}{300}\right)^{-n}} \right) / N \right]^2} \quad (5)$$

Where  $N = [0.75 - 1.27 \log F_c]$  and  $F_c$  is the broadening factor at the centre of the fall-off curve.

135 As discussed in some detail in the first part of our studies of the title reaction (Amedro et al., 2019), the low- or high-pressure rate constants for the title reaction ( $k_0$  and  $k_\infty$ ) are not well defined by existing data sets, which do not deliver sufficiently accurate rate coefficient at very low pressures ( $< 1$  mbar) or at very high pressures ( $> 500$  bar). Studies in which  $k_\infty$  has been derived from rates of vibrational relaxation of OH (Smith and Williams, 1985; D'Ottone et al., 2005), return values of  $k_\infty$  that provide some constraint on its value, but the associated uncertainty is too large to consider this parameter well defined.

140 In our first paper, Amedro et al. (2019) describe highly accurate measurements of  $k_1$  over a wide range temperatures and pressures in the fall-off regime. From measurements of  $k_1$  in  $\text{N}_2$  bath-gas, we retrieved values of  $k_0$  and  $k_\infty$  of  $2.6 \times 10^{-30} \text{ cm}^6 \text{ molecule}^{-2} \text{ s}^{-1}$  and  $6.3 \times 10^{-11} \text{ cm}^3 \text{ molecule}^{-1} \text{ s}^{-1}$ , respectively, by fixing  $F_c$  to a value of 0.39 which has theoretical basis (Cobos and Troe, 2003). The reasons for choosing this value of  $F_c$  are discussed in Amedro et al. (2019). Note that whereas  $k_0$  is dependent on the bath-gas used, at the high-pressure limit,  $k_\infty$  should be the same in  $\text{N}_2$ ,  $\text{O}_2$ , He or  $\text{H}_2\text{O}$  bath gases.

145 In Fig.1 we display pressure dependent rate coefficients (solid, black squares) obtained in He bath-gas at 292 K. The black line is a fit (Eqn. 4) to our data with  $k_\infty$  fixed to  $6.3 \times 10^{-11} \text{ cm}^3 \text{ molecule}^{-1} \text{ s}^{-1}$  and  $n = 0$  as derived from an extensive dataset obtained using  $\text{N}_2$  bath-gas (Amedro et al., 2019). For this dataset, the best fit is obtained with  $F_c = 0.32$ , and  $k_0^{\text{He}} = 1.4 \times 10^{-30} \text{ cm}^6 \text{ molecule}^{-2} \text{ s}^{-1}$ . When using  $F_c = 0.39$  (i.e. same value as that obtained in  $\text{N}_2$  bath-gas), the fit slightly overestimates ( $\sim 5\%$ ) the measurements at pressures above  $\sim 300$  Torr whereas it underestimates by 10 % at lower pressures (Fig. S2). We note that using a higher  $F_c = 0.39$  resulted in a lower value of  $k_0^{\text{He}}$  equal to  $1.0 \times 10^{-30} \text{ cm}^6 \text{ molecule}^{-2} \text{ s}^{-1}$ . The T-dependence factor in He,  $m(\text{He})$ , was determined to be 3.1 over the temperature range from 277 to 332 K (Table 1 and Figure S6).

150

The high precision of our measurements in He and N<sub>2</sub> indicates that different broadening factors ( $F_c$ ) are required to interpret the pressure dependence of  $k_1$  obtained in N<sub>2</sub> and He. This can be rationalized by considering that  $F_c$  is the product of strong-collision ( $F_c^{SC}$ ) and weak-collision ( $F_c^{WC}$ ) components (Eqn. 6-8) (Gilbert et al., 1983; Troe, 1983; Troe and Ushakov, 2011)

$$F_c \approx F_c^{SC} F_c^{WC} \quad (6)$$

$$F_c^{SC} \approx S_K^{-0.62} \approx \left(1 + \frac{r}{2}\right)^{-0.62} \quad (7)$$

$$F_c^{WC} \approx \beta_c^{0.14} \quad (8)$$

Here,  $S_K$  is the Kassel parameter and  $r$  is the total number of external rotational modes of the reactants (equal to 5 in the reaction between OH and NO<sub>2</sub>) and  $\beta_c$  is the collision efficiency. While the strong collision component is independent of bath gas ( $F_c^{SC} \approx 0.46$  for the title reaction) a change in  $F_c^{WC}$  due to a lower collision efficiency ( $\beta_c$ ) of He relative to N<sub>2</sub> is likely.

The collision efficiency for N<sub>2</sub> which was used to calculate  $F_c = 0.39$  was  $\beta_c(\text{N}_2) \approx 0.3$  (Troe, 2001). The value of  $F_c = 0.32$  from our He data implies  $\beta_c(\text{He}) \approx 0.08$ , a factor 3.7 times lower than  $\beta_c(\text{N}_2)$ . A large difference in collision efficiency between N<sub>2</sub> and He is consistent with theoretical calculations (Glänzer and Troe, 1974; Troe, 2001; Golden et al., 2003).

In Fig 1, we also compare our measurements of  $k_1$  in He with data collected in the same pressure range using similar techniques.

The three first measurements (Morley and Smith, 1972; Anastasi and Smith, 1976; Wine et al., 1979) used flash photolysis of H<sub>2</sub>O as a OH precursor with detection of OH by resonance fluorescence. Morley and Smith (1972) reported rate coefficients at pressures of 20 to 280 Torr at room temperature with the NO<sub>2</sub> concentration calculated manometrically. Our parametrisation agrees within the combined uncertainty of both measurements (Figure S3). Anastasi and Smith (1976) reported one value of  $k_1$  at 25 Torr He which is  $\approx 20\%$  lower than our measurement. Wine et al. (1979) presented values of  $k_1$  at 3 pressures of He.

The agreement with our parameterisation at the lowest two pressures is excellent but a deviation of  $\approx 20\%$  is observed at the highest pressure (Figure S4). As both studies measured NO<sub>2</sub> concentrations using optical absorption at 365 nm, the  $\approx 20\%$  difference is significant. Most recently, D'Ottone et al. (2001) reported rate coefficients from 30 to 600 Torr He using a very similar approach to ours i.e. PLP-LIF technique with in situ measurements of NO<sub>2</sub> by absorption at 365 nm. The disagreement (up to 40%) between our measurements and theirs exceed the combined reported uncertainty (Figure S5). While it is unclear what could have caused the discrepancy, we note that the data of D'Ottone et al. (2001) are significantly more scattered and do not describe a smooth increase in rate coefficient with pressure as expected from termolecular reactions in the fall-off regime. This would appear to indicate an underestimation of the total uncertainty in their study.

Figure 2 extends the pressure range to additionally display data obtained in low pressure flow-tubes (Westenberg and Dehaas, 1972; Anderson et al., 1974; Erler et al., 1977; Anderson, 1980) and the high-pressure measurements by Hippler et al. (2006).

At low pressures our data is in excellent agreement (within 10%) with the data of Erler et al. (1977) but predict values  $\approx 40\%$  lower than those reported by Westenberg and Dehaas (1972) and Anderson (1980). The data of Anderson et al. (1974) display a large intercept ( $4.9 \times 10^{-14} \text{ cm}^3 \text{ molecule}^{-1} \text{ s}^{-1}$ ) at zero pressure, which is attributed to a second-order heterogeneous removal rate constant. As indicated in a critical assessment of the low-pressure data by Amedro et al. (2019) it is unclear whether one can simply subtract a constant value equal to the intercept (obtained from a linear fit) to each data point. If we were to do so, the work by Anderson et al. (1974) would be in very good agreement with the low pressure study by Erler et al. (1977) as well as with our parametrisation extended to low pressures. Additionally, Amedro et al. (2019) demonstrated that, owing to the large, asymmetric broadening of fall-off for this reaction the assumption that the rate coefficient is in the low pressure limit at N<sub>2</sub> pressures of  $0.5 \text{ Torr} < p < 10 \text{ Torr}$  is invalid and leads to underestimation of  $k_0$ . This observation is still true of datasets obtained at low pressures of He, so that while very good agreement is observed between our parametrisation and individual rate coefficients obtained between 3 and 8 Torr of He, reported values of  $k_0^{\text{He}}$  are 40 % lower than our values obtained from the fall-off analysis. As indicated in Fig. 2, our parametrisation of  $k_1$  in He is in very good agreement with the high pressure data reported by Hippler et al. (2006).

### 3.2 Influence of H<sub>2</sub>O on $k_1$

As mentioned above, the effect of water vapour on  $k_1$  was determined in mixtures of H<sub>2</sub>O with both N<sub>2</sub> and He. This is because the vapour pressure of H<sub>2</sub>O at room temperature ( $\approx 17$  Torr at 293 K) is too low to enable experiments in pure H<sub>2</sub>O bath gas to be conducted using our instrument. The measurements were performed at low density ( $[M] = 1.6 \times 10^{18}$  molecule cm<sup>-3</sup>; 50 Torr at 293 K) where the relative increase of  $k_1$  in the presence of H<sub>2</sub>O is pronounced, resulting in greater accuracy in the determination of  $k_0^{\text{H}_2\text{O}}$ . Experimental data on the influence of H<sub>2</sub>O on  $k_1$  was obtained in N<sub>2</sub>-H<sub>2</sub>O and He-H<sub>2</sub>O mixtures by varying the H<sub>2</sub>O mixing ratio,  $x_{\text{H}_2\text{O}}$ , from 0.05 to 0.27 ( $[\text{H}_2\text{O}] = 0.9 - 4.5 \times 10^{17}$  molecule cm<sup>-3</sup>) while keeping the total pressure constant at 50 Torr. Under these conditions, the addition of H<sub>2</sub>O resulted in an increase in  $k_1$  up to a factor of two as illustrated by the datasets of Fig. 3 in which the increase in slope as more water-vapour is added is proportional to the increase in  $k_1$  (Eqn. 2). At the highest concentration of water vapour ( $4.5 \times 10^{17}$  molecule cm<sup>-3</sup>) the rate coefficient in He-H<sub>2</sub>O increased by > factor 3 compared to that obtained in pure He (see Table 1).

In order to determine the temperature dependence of the enhancement in  $k_1$  caused by the presence of water, the experiments in He were carried out at 3 different temperatures (277, 291 and 332 K). The values of  $k_1$  obtained from these experiments are plotted versus the mole-fraction of H<sub>2</sub>O in Fig. 4b. At the pressures used in our experiments,  $k_1$  displays fall-off, precluding direct measurement of  $k_0^{\text{H}_2\text{O}}$ .

~~In other words,~~ The total rate constant measured in e.g. a H<sub>2</sub>O-N<sub>2</sub> bath gas is not equal to the sum of the individual rate constants calculated from the mixing ratios of N<sub>2</sub> and H<sub>2</sub>O i.e.  $k_{\text{N}_2\text{-H}_2\text{O}} \neq k_{\text{N}_2} + k_{\text{H}_2\text{O}}$ .  $k_{\text{N}_2\text{-H}_2\text{O}}$  is only equal to the sum of  $k_{\text{N}_2}$  and  $k_{\text{H}_2\text{O}}$  at the low pressure limit ( $\ll 1$  Torr in the case of the OH reaction with NO<sub>2</sub>) and under certain conditions where gas mixtures are composed of strong colliders and/or have similar collision efficiencies (Troe, 1980; Burke and Song, 2017). Additionally, at the high-pressure end of the fall-off curve, the rate coefficient is independent of bath gas composition. To be able to make a reasonable prediction of this effect under atmospheric conditions where the mole fraction of water vapour,  $x_{\text{H}_2\text{O}}$ , can be as large as 0.05, we analysed our measurements using two different approaches to determine  $k_0^{\text{H}_2\text{O}}$ . In the first case, the low pressure rate constant in a N<sub>2</sub>-H<sub>2</sub>O mixture is defined as the sum of two individual low pressure limit rate constants,

$$k(P, T) = \frac{\left(x_{\text{N}_2} k_0^{\text{N}_2} \left(\frac{T}{300}\right)^{-m} + x_{\text{H}_2\text{O}} k_0^{\text{H}_2\text{O}} \left(\frac{T}{300}\right)^{-o}\right) [M] k_\infty \left(\frac{T}{300}\right)^{-n}}{\left(x_{\text{N}_2} k_0^{\text{N}_2} \left(\frac{T}{300}\right)^{-m} + x_{\text{H}_2\text{O}} k_0^{\text{H}_2\text{O}} \left(\frac{T}{300}\right)^{-o}\right) [M] + k_\infty \left(\frac{T}{300}\right)^{-n}} F \quad (9)$$

where  $x_{\text{N}_2}$  and  $x_{\text{H}_2\text{O}}$  are the mixing ratio for N<sub>2</sub> and H<sub>2</sub>O respectively,  $k_0^{\text{N}_2}$  and  $k_0^{\text{H}_2\text{O}}$  are low-pressure limiting rate constants (units of cm<sup>6</sup> molecule<sup>-2</sup> s<sup>-1</sup>) for pure N<sub>2</sub> and H<sub>2</sub>O,  $k_\infty$  is the high-pressure limit rate constant (units of cm<sup>3</sup> molecule<sup>-1</sup> s<sup>-1</sup>),  $T$  is the temperature in Kelvin,  $[M]$  is the molecular density (molecule cm<sup>-3</sup>) and  $m$ ,  $n$  and  $o$  are dimensionless temperature exponents.

The broadening factor,  $F$ , is:

$$\log F = \frac{\log F_c}{1 + \left[ \log \left( \frac{\left(x_{\text{N}_2} k_0^{\text{N}_2} \left(\frac{T}{300}\right)^{-m} + x_{\text{H}_2\text{O}} k_0^{\text{H}_2\text{O}} \left(\frac{T}{300}\right)^{-o}\right) [M]}{k_\infty \left(\frac{T}{300}\right)^{-n}} \right) / N \right]^2} \quad (10)$$

Where  $N = [0.75 - 1.27 \log F_c]$  and  $F_c$  is the broadening factor at the centre of the fall-off curve.

In the second approach, we follow Burke and Song (2017) where, additionally to the low pressure limiting rate coefficients, the broadening factors for each bath gas are also mixed linearly and  $\log F^{\text{N}_2\text{-H}_2\text{O}}$  is defined as

$$\log F^{\text{N}_2\text{-H}_2\text{O}} = \tilde{X}_{\text{N}_2} \log F^{\text{N}_2} + \tilde{X}_{\text{H}_2\text{O}} \log F^{\text{H}_2\text{O}} \quad (11)$$

$$\text{where } \tilde{X}_{\text{N}_2} = \frac{x_{\text{N}_2} k_0^{\text{N}_2} \left(\frac{T}{300}\right)^{-m} [M]}{\left(x_{\text{N}_2} k_0^{\text{N}_2} \left(\frac{T}{300}\right)^{-m} + x_{\text{H}_2\text{O}} k_0^{\text{H}_2\text{O}} \left(\frac{T}{300}\right)^{-o}\right) [M]}; \tilde{X}_{\text{H}_2\text{O}} = \frac{x_{\text{H}_2\text{O}} k_0^{\text{H}_2\text{O}} \left(\frac{T}{300}\right)^{-m} [M]}{\left(x_{\text{N}_2} k_0^{\text{N}_2} \left(\frac{T}{300}\right)^{-m} + x_{\text{H}_2\text{O}} k_0^{\text{H}_2\text{O}} \left(\frac{T}{300}\right)^{-o}\right) [M]} \quad (12)$$

$$\log F_c^{N_2} = \frac{\log F_c^{N_2}}{1 + \left[ \log \left( \frac{\left( x_{N_2} k_0^{N_2} \left( \frac{T}{300} \right)^{-m} + x_{H_2O} k_0^{H_2O} \left( \frac{T}{300} \right)^{-o} \right) [M]}{k_\infty \left( \frac{T}{300} \right)^{-n}} \right) / (0.75 - 1.27 \log F_c^{N_2}) \right]^2} \quad (13)$$

$$\log F_c^{H_2O} = \frac{\log F_c^{H_2O}}{1 + \left[ \log \left( \frac{\left( x_{N_2} k_0^{N_2} \left( \frac{T}{300} \right)^{-m} + x_{H_2O} k_0^{H_2O} \left( \frac{T}{300} \right)^{-o} \right) [M]}{k_\infty \left( \frac{T}{300} \right)^{-n}} \right) / (0.75 - 1.27 \log F_c^{H_2O}) \right]^2} \quad (14)$$

where  $F_c^{N_2}$  and  $F_c^{H_2O}$  are the broadening factor at the centre of the fall off curve for  $N_2$  and  $H_2O$ .

235 In the case where two bath gases have identical (or very similar) values of  $F_c$ , the two approaches result in identical predictions and the first approach will be preferred for its simplicity. This is the case for  $N_2$  and  $H_2O$  bath gases. However, when two bath-gases have significantly different values of  $F_c$  (as is the case for He- $H_2O$  mixtures, see below) the second approach provides a more accurate parameterisation.

### 3.2.1 Parameterisation of $k_1$ from data obtained in $N_2$ - $H_2O$ and He- $H_2O$ bath gases

240 Values of  $k_1$  obtained in  $N_2$ - $H_2O$  and He- $H_2O$  bath gases are listed in Table 2. Each rate coefficient obtained in  $N_2$ - $H_2O$  bath gas was defined by 5 parameters: the mixing ratio of  $N_2$  and  $H_2O$  ( $x_{N_2}$  and  $x_{H_2O}$ ) the overall rate coefficient ( $k_1$ ) the molecular density  $[M]$  and the temperature  $T$ . We performed a multivariate fit of the  $N_2$ - $H_2O$  dataset with  $k_0^{H_2O}$  as variable, all other parameters fixed with:  $k_\infty = 6.3 \times 10^{-11} \text{ cm}^3 \text{ molecule}^{-1} \text{ s}^{-1}$ ,  $k_0^{N_2} = 2.6 \times 10^{-30} \text{ cm}^6 \text{ molecule}^{-2} \text{ s}^{-1}$  and  $m = 3.6$  as derived in Amedro et al. (2019),  $o$  was fixed to 3.4 (see below) and  $F_c$  was held at 0.39 making the assumption that the broadening factors at the

245 centre of the fall-off curve for  $H_2O$  and  $N_2$  were identical. The fit to the data returned  $k_0^{H_2O} = (15.9 \pm 0.7) \times 10^{-30} \text{ cm}^6 \text{ molecule}^{-2} \text{ s}^{-1}$  where the uncertainty is  $2\sigma$  (statistical only). The solid black line on the upper panel of Fig. 4a represents the parametrisation for a varying fraction of  $H_2O$  in  $N_2$  at a total pressure of 50 Torr using the parameters given above. Equating  $F_c^{H_2O}$  and  $F_c^{N_2}$  simplifies the analysis, though it is likely that  $F_c^{H_2O} > F_c^{N_2}$  as the collision efficiency ( $\beta_c$ ) is likely to be larger for  $H_2O$  than for  $N_2$ . We found that the He- $H_2O$  data cannot be modelled assuming the same  $F_c$  for both He and  $H_2O$  bath gas

250 and the approach of Burke and Song (2017) was therefore preferred. In order to analyse the data we fixed the following parameters:  $k_0^{H_2O} = 15.9 \times 10^{-30} \text{ cm}^6 \text{ molecule}^{-2} \text{ s}^{-1}$ ,  $F_c^{H_2O} = 0.39$ ,  $F_c^{He} = 0.32$  and  $k_0^{He} = 1.4 \times 10^{-30} \text{ cm}^6 \text{ molecule}^{-2} \text{ s}^{-1}$  and  $m = 3.1$  to derive  $o = (3.4 \pm 0.8)$  ( $2\sigma$ , statistical only), which describes the **temperature dependence** of the low pressure limit in  $H_2O$  as depicted in Fig. 4b.

There is clearly some uncertainty related to the arbitrary use of  $F_c^{H_2O} = 0.39$ . For example, if we were to use analyse the data

255 in  $N_2$ - $H_2O$  using  $F_c^{H_2O} = 0.6$  and the linear mixing method we retrieve  $k_0^{H_2O} = 10 \times 10^{-30} \text{ cm}^6 \text{ molecule}^{-2} \text{ s}^{-1}$ , which is  $\approx 50\%$  lower than our preferred value. The effect of the different analyses can be assessed by comparing the predicted impact of  $H_2O$  on  $k_1$  at 80% relative humidity, 1000 mbar and 313 K. If we set  $F_c^{H_2O} = 0.39$  we predict that the effect of  $H_2O$  is to increase  $k_1$  by 15% while choosing  $F_c^{H_2O} = 0.6$  results in an increase of 20%. Theoretical calculation of the relative values of  $F_c$  in  $N_2$ ,  $O_2$  and  $H_2O$  bath gases input would be useful to reduce this uncertainty. Our data indicate a significant, positive trend in  $k_1$  when

260 adding  $H_2O$ . As discussed above, more efficient energy transfer from  $[HO-NO_2]^\#$  in collision with  $H_2O$  compared to  $N_2$  is intuitive and supported by the present dataset as well as that of Simonaitis and Heicklen (1972) who derived  $k_0^{H_2O} = 11 \times 10^{-30} \text{ cm}^6 \text{ molecule}^{-2} \text{ s}^{-1}$ . Given the complexity of the analysis, this may be considered to be in good agreement. This result is however not consistent with the observations of D'Ottone et al. (2001) who report no significant change in  $k_1$  in 150 Torr of He when adding either 10 or 20 Torr of  $H_2O$  and is completely at odds with the conclusions of Sadanaga et al. (2006), who report a

265 reduction in  $k_1$  (by 18%) when adding 29.1 mbar of  $H_2O$  at atmospheric pressure. If our value for  $k_0^{H_2O}$  is correct, D'Ottone et al. (2001) should have seen an increase in  $k_1$  of  $\approx 55\%$  and Sadanaga et al. (2006) should have observed an increase of  $\approx 5\%$ .

A potential explanation for the very divergent observations of the effect of H<sub>2</sub>O is the heterogeneous loss of NO<sub>2</sub> when adding H<sub>2</sub>O. We tested for NO<sub>2</sub> loss in a set of experiments in which NO<sub>2</sub> and H<sub>2</sub>O were monitored simultaneously while systematically varying the amount of H<sub>2</sub>O. Our results indicated a reduction in the concentration of NO<sub>2</sub> by up to  $\approx 20\%$  as we  
270 increased the concentration of H<sub>2</sub>O up to  $4.5 \times 10^{17}$  molecule cm<sup>-3</sup>. Unless NO<sub>2</sub> is monitored in-situ (as in our experiments), 20% loss of NO<sub>2</sub> would lead to a similar size reduction in the OH decay constant and thus an underestimation of the rate coefficient. A fractional loss of NO<sub>2</sub> of this magnitude would explain why Sadanaga et al. (2006) found an apparent reduction in  $k_1$  when adding H<sub>2</sub>O.

However, the situation becomes more complex if NO<sub>2</sub> is converted to trace gases that are reactive towards OH. For this reason,  
275 we performed an additional experiment to investigate whether NO<sub>2</sub> was converted via reaction with H<sub>2</sub>O on surfaces to HONO and/or HNO<sub>3</sub>. Note that conversion of NO<sub>2</sub> to HONO at low pressures (e.g. 50 Torr) would result in an increase in the OH decay constant ( $k_{\text{OH}+\text{HONO}} > k_{\text{OH}+\text{NO}_2}$ ), whereas conversion of NO<sub>2</sub> to HNO<sub>3</sub> would result in a decrease ( $k_{\text{OH}+\text{HNO}_3} < k_{\text{OH}+\text{NO}_2}$ ).

In order to test for the presence of HONO, we modified the broadband absorption set-up by replacing the halogen lamp with a deuterium lamp, allowing us to detect HONO around 350 nm as well as NO<sub>2</sub>. The optical absorption of NO<sub>2</sub> and HONO  
280 (340 – 380 nm) was monitored in a flow of NO<sub>2</sub> ( $1.7 \times 10^{15}$  cm<sup>-3</sup>) at 50 Torr He in the absence and presence of H<sub>2</sub>O ([H<sub>2</sub>O] =  $4.5 \times 10^{17}$  molecule cm<sup>-3</sup>, the maximum concentration used in this work). A depletion in NO<sub>2</sub> of 21% ( $3.7 \times 10^{14}$  molecule cm<sup>-3</sup>) was observed when H<sub>2</sub>O was added. An analysis of the spectra with and without H<sub>2</sub>O (Fig. S7) enabled us to establish an upper limit to the HONO concentration of  $\approx 1 \times 10^{13}$  molecule cm<sup>-3</sup>, which would corresponds to just 3% of the NO<sub>2</sub> lost. At this concentration, HONO does not significantly increase the loss-rate of OH (< 3% using a rate coefficient for reaction of OH  
285 with HONO of  $6.0 \times 10^{-12}$  cm<sup>3</sup> molecule<sup>-1</sup> s<sup>-1</sup> (IUPAC, 2019)). In the same experiment, we also recorded the optical density at 185 nm where H<sub>2</sub>O, NO<sub>2</sub> and HNO<sub>3</sub> all absorb. Despite the large HNO<sub>3</sub> absorption cross-section at this wavelength ( $1.6 \times 10^{-17}$  cm<sup>2</sup> molecule<sup>-1</sup>, Dulitz et al. (2018)) we found no evidence for HNO<sub>3</sub> formation, indicating that the NO<sub>2</sub> lost was not converted to gas-phase HNO<sub>3</sub>. Given its great affinity for glass in the presence of H<sub>2</sub>O, we expect that any HNO<sub>3</sub> formed is strongly partitioned to the walls of the reactor. The tests indicate that, on the time scales of our experiments, NO<sub>2</sub> is lost  
290 irreversibly on the humidified walls of our experiment. The maximum concentration of H<sub>2</sub>O used in this experiment,  $4.5 \times 10^{17}$  molecule cm<sup>-3</sup>, corresponding to a relative humidity of 80% (at 292 K) so that H<sub>2</sub>O condensation is not expected.

It is difficult to establish whether our observations of significant NO<sub>2</sub> loss can explain the result of D'Ottone et al. (2001), who did not observe an enhancement in  $k_1$ . D'Ottone et al. (2001) did not state whether, in their experiments, NO<sub>2</sub> and H<sub>2</sub>O were monitored simultaneously. Also, our observed loss of NO<sub>2</sub> is not necessarily transferable to other studies as the heterogeneous  
295 loss of NO<sub>2</sub> will vary from one experimental set-up to the next, as residence times and surface areas may vary substantially.

A very simple calculation serves to illustrate the role of water vapour as a third-body quencher for the title reaction. We consider e.g. the tropical boundary layer with a **temperature** of 30 °C and a relative humidity of 80% at a total pressure of 1 bar. The pressure of water vapour is 34 mbar, those of O<sub>2</sub> and N<sub>2</sub> are then **210** and **756** mbar, respectively. A rough contribution of each quenching gas to the overall rate coefficient can be calculated from the respective low-pressure rate coefficients. For  
300 N<sub>2</sub>, O<sub>2</sub> and H<sub>2</sub>O these are (in units of 10<sup>-30</sup> cm<sup>3</sup> molecule<sup>-1</sup> s<sup>-1</sup>) 2.6, 2.0 and 15.9. **Water vapour is therefore a factor  $\approx 8$  more efficient than O<sub>2</sub>, and a factor  $\approx 6$  more efficient than N<sub>2</sub> as a quencher of the HO-NO<sub>2</sub> intermediate, which is qualitatively consistent with known strong binding (40 kJ mol<sup>-1</sup>) in the HNO<sub>3</sub>-H<sub>2</sub>O complex (Tao et al., 1996).**

For our tropical boundary layer case-study, in which the O<sub>2</sub> pressure is only a factor of six greater than that of H<sub>2</sub>O, we calculate that H<sub>2</sub>O contributes more to the rate coefficient of the title reaction than does O<sub>2</sub>. Clearly, the neglect of including the  
305 quenching effect of H<sub>2</sub>O leads to underestimation (**in the boundary layer**) of the rate coefficient for this centrally important atmospheric reaction.

In order to assess both the effect of H<sub>2</sub>O (this work) and the new parameterisation for  $k_1$  in N<sub>2</sub> and O<sub>2</sub> bath-gases presented in first part of this study (Amedro et al., 2019), we have used a 3D chemical transport model (EMAC, see below) to explore the impact on a global scale.



### 310 3.3. Atmospheric modelling of the OH + NO<sub>2</sub> reaction including the effect of water vapour

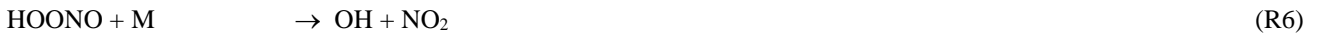
The EMAC (ECHAM-MESSy Atmospheric Chemistry) model employed is a numerical chemistry and climate simulation system (Jöckel et al., 2006; Jöckel et al., 2010) using the 5th generation European Centre Hamburg general circulation model (ECHAM5, Roeckner et al. (2006)) as core atmospheric general circulation model. For the present study we applied EMAC (ECHAM5 version 5.3.02, MESSy version 2.53.0) in the T42L47MA-resolution, i.e. with a spherical truncation of T42 (corresponding to a quadratic Gaussian grid of approx. 2.8 by 2.8 degrees in latitude and longitude) with 47 vertical hybrid pressure levels up to 0.01 hPa. The model has been weakly nudged in spectral space, nudging temperature, vorticity, divergence and surface pressure (Jeuken et al., 1996). The chemical mechanism scheme adopted (MOM, Mainz Organic Mechanism) includes oxidation of isoprene, saturated and unsaturated hydrocarbons, including terpenes and aromatics (Sander et al., 2019). Further, tracer emissions and model set-up are similar to the one presented in Lelieveld et al. (2016a). EMAC model predictions have been evaluated against observations on several occasions (Pozzer et al., 2010; de Meij et al., 2012; Elshorbany et al., 2014; Yoon and Pozzer, 2014): For additional references, see <http://www.messy-interface.org>. For this study, EMAC was used in a chemical-transport model (CTM mode) (Deckert et al., 2011), i.e., by disabling feedbacks from photochemistry on radiation and dynamics. Two years were simulated (2009-2010), with the first year used as spin-up time. The following parameterisation of  $k_1$  was implemented in EMAC; values of each parameter are listed in Table 3.

$$k_1(P, T) = \frac{\left(x_{\text{N}_2}k_0^{\text{N}_2}\left(\frac{T}{300}\right)^{-m} + x_{\text{O}_2}k_0^{\text{O}_2}\left(\frac{T}{300}\right)^{-q} + x_{\text{H}_2\text{O}}k_0^{\text{H}_2\text{O}}\left(\frac{T}{300}\right)^{-o}\right)Mk_\infty\left(\frac{T}{300}\right)^{-n}}{\left(x_{\text{N}_2}k_0^{\text{N}_2}\left(\frac{T}{300}\right)^{-m} + x_{\text{O}_2}k_0^{\text{O}_2}\left(\frac{T}{300}\right)^{-q} + x_{\text{H}_2\text{O}}k_0^{\text{H}_2\text{O}}\left(\frac{T}{300}\right)^{-o}\right)M+k_\infty\left(\frac{T}{300}\right)^{-n}}F \quad (15)$$

The broadening factor,  $\log F$ , is:

$$\log F = \frac{\log F_c}{1 + \left[ \log \left( \frac{\left(x_{\text{N}_2}k_0^{\text{N}_2}\left(\frac{T}{300}\right)^{-m} + x_{\text{O}_2}k_0^{\text{O}_2}\left(\frac{T}{300}\right)^{-q} + x_{\text{H}_2\text{O}}k_0^{\text{H}_2\text{O}}\left(\frac{T}{300}\right)^{-o}\right)M}{k_\infty\left(\frac{T}{300}\right)^{-n}} \right) / [0.75 - 1.27 \log F_c] \right]^2} \quad (16)$$

As described in Section 1, the reaction between OH and NO<sub>2</sub> forms not only HNO<sub>3</sub> but also HOONO. HOONO decomposes rapidly at typical boundary layer temperatures but is long lived with respect to thermal dissociation at the temperatures found in the upper troposphere and lower stratosphere (UTLS).



The rate constant ( $k_6$ ) for thermal decomposition of HOONO was calculated from the channel specific rate coefficient for its formation ( $k_1\alpha$ ) and an equilibrium coefficient:  $k_6 = k_1\alpha / K_{\text{eq}}$ , where  $K_{\text{eq}} = 3.5 \times 10^{-27} \exp(10135/T)$  (Burkholder et al., 2015; IUPAC, 2019) based on the analysis of (Golden et al., 2003). The branching ratio to HOONO formation ( $\alpha$ ) was adapted from the present IUPAC recommendations for  $k_{1a}$  and  $k_{1b}$  which were derived from experimental work (Hippler et al., 2006; Mollner et al., 2010) and theoretical analysis (Troe, 2012). The IUPAC recommendations were augmented with a pressure independent HOONO yield of 0.035 to better represent the dataset of Mollner et al. (2010) who detected HOONO directly at room temperature. **We assume  $\alpha$  is independent of water vapour.** The expression used and a plot of  $\alpha$  at different temperatures and pressures is given in Fig. S8 of the supplementary information.

In the absence of experimental data on the reactions of HOONO with OH or on its photolysis, we follow the approach of Golden and Smith (2000) and set these equal to those for HO<sub>2</sub>NO<sub>2</sub>:



In Fig. 5, we illustrate the global impact (annual average) of H<sub>2</sub>O-vapour on the rate coefficient. We plot the fractional reduction in  $k_1$  at the Earth's surface when setting  $x_{\text{H}_2\text{O}}$  to zero rather than using the EMAC global water-vapour fields. We focus on the boundary layer as the H<sub>2</sub>O concentration is largest here and decreases rapidly with altitude.



As expected, the greatest effect is found in warm, tropical regions where neglecting the impact of water vapour results in an average underestimation of the rate coefficient by up to  $\approx 8\%$ . At higher/lower latitudes the effect is diminished and water vapour accounts for only 3-4 % of the overall rate coefficient at  $40^\circ$  N/S. **The presence of water vapour does not impact on values of  $k_1$  above the boundary layer.**

Our experimental data do not give insight into whether the  $\text{H}_2\text{O}$ -induced enhancement in  $k_1$  is accompanied by a change in the branching ratio to favour either  $\text{HNO}_3$  or  $\text{HOONO}$ . However, as the formation of  $\text{HOONO}$  is favoured at high pressures (more effective collisional deactivation) it is possible that the  $\text{HOONO}$  yield may be enhanced relative to  $\text{HNO}_3$  in the presence of  $\text{H}_2\text{O}$ . If this is the case, the increase in rate coefficient at high water vapour levels (e.g. in the tropical lower troposphere) may be to some extent offset by the subsequent thermal dissociation of  $\text{HOONO}$  in these warm regions.

As described by Amedro et al. (2019) (Fig. 1 of their manuscript) two expert panels (IUPAC, NASA) evaluating kinetic data for use in atmospheric modelling fail to reach consensus for the title reaction, with the preferred rate coefficients differing by as much as 50% in the cold UTLS. For this reason we have calculated values of  $\frac{k_1^{\text{NASA}}}{k_1^{\text{this work}}}$  and  $\frac{k_1^{\text{IUPAC}}}{k_1^{\text{this work}}}$  at different altitudes and latitudes (i.e. at different temperatures and pressures). We parameterized the rate coefficient using the expressions given in this work (Eqn. 15, Table 3) and in the latest evaluations of IUPAC ( $k_1$  last evaluated in 2017 (IUPAC, 2019)) and NASA (last evaluation published in 2015 (Burkholder et al., 2015)). As displayed in Fig. 6, values of  $\frac{k_1^{\text{NASA}}}{k_1^{\text{this work}}}$  and  $\frac{k_1^{\text{IUPAC}}}{k_1^{\text{this work}}}$  vary greatly with pressure and temperature and thus altitude. The NASA recommendations are always slightly lower but in good agreement ( $\leq 10\%$ ) for most of the troposphere, with larger differences ( $(\frac{k_1^{\text{NASA}}}{k_1^{\text{this work}}})$  always  $< 1$ ) only observed in the lower and mid-stratosphere. At altitudes above  $\approx 30$  km the ratio decreases to  $\approx 0.8$ . A comparison with the rate coefficient derived from the IUPAC parameterization, shows that  $\frac{k_1^{\text{IUPAC}}}{k_1^{\text{this work}}}$  varies from  $\approx 0.9$  at the surface to  $\approx 1.1$  at the tropopause but increases to  $> 1.3$  at the low pressures and temperatures that reign at 30 km and above. At high altitudes (low pressure and temperature) the rate coefficients that the evaluation panels recommend are strongly biased by choice of the rate coefficient (and its temperature dependence) at the low pressure limit. As discussed by Amedro et al. (2019) the available experimental data at low pressures and temperature are not of sufficient accuracy to use as basis for recommendation of  $k_0$  and this is reflected in the highly divergent values of  $k_1$  under these conditions.

As mentioned above, the atmospheric  $\text{HNO}_3 / \text{NO}_2$  ratio is expected to be highly sensitive to the rate coefficient  $k_1$ , with an increase in  $k_1$  resulting in an increase in the  $\text{HNO}_3 / \text{NO}_2$  ratio and vice versa. The  $\text{HNO}_3 / \text{NO}_2$  ratio also depends on the concentration of OH and thus the effect of using different values of  $k_1$  will be most apparent in regions where the greatest OH concentrations are found, i.e. at low latitudes. At higher latitudes, especially in winter months where solar insolation is weak and OH levels are relatively low, the  $\text{HNO}_3 / \text{NO}_2$  ratio will also be impacted by nighttime conversion of  $\text{NO}_2$  to  $\text{N}_2\text{O}_5$  and finally, via heterogeneous hydrolysis, to  $\text{HNO}_3$ . In Fig. 7 we plot zonally and yearly averaged model values of  $\frac{\text{HNO}_3}{\text{NO}_2}(\text{IUPAC}) / \frac{\text{HNO}_3}{\text{NO}_2}(\text{this work})$  in the upper panel and  $\frac{\text{HNO}_3}{\text{NO}_2}(\text{NASA}) / \frac{\text{HNO}_3}{\text{NO}_2}(\text{this work})$  in the lower panel. Compared to the present parameterization of  $k_1$ , the IUPAC evaluation returns  $\text{HNO}_3 / \text{NO}_2$  ratios that are between 0.9 and 1 throughout most of the lower and free-troposphere (up to  $\approx 5$  km) and larger  $\text{HNO}_3 / \text{NO}_2$  ratios (factor of 1.1 to 1.15) above  $\approx 10$  km especially at the tropical tropopause. The divergence between the  $\text{HNO}_3 / \text{NO}_2$  ratios increases as we move further into the stratosphere with  $\frac{\text{HNO}_3}{\text{NO}_2}(\text{IUPAC}) / \frac{\text{HNO}_3}{\text{NO}_2}(\text{this work})$  as large as 1.2 to 1.3 above 25 km. At the same time,  $\text{NO}_x$  levels ( $\text{NO}_x = \text{NO} + \text{NO}_2$ ) decrease by a factor  $\approx 0.95$  (see Fig. S9 of the supplementary information). When we compare our parameterization with that of the NASA panel, the picture is largely reversed (lower panel). Again, we find reasonable agreement in the  $\text{HNO}_3 / \text{NO}_2$  ratio in the lowermost atmosphere, but in this case lower values (0.8 to 0.9) in the lower stratosphere which are accompanied by a factor 1.06 change in  $\text{NO}_x$  concentrations (Fig. S9). For both the NASA and IUPAC parameterizations, the largest differences in the  $\text{HNO}_3 / \text{NO}_2$  ratio compared to the present study are found higher in the atmosphere. The modelling studies confirm the

simple calculation of Amedro et al. (2019) (see Fig. 1 of their paper), showing that the IUPAC and NASA parameterizations result in very different values of  $k_1$  in some parts of the atmosphere and will result in divergent predictions of partitioning of reactive nitrogen between  $\text{NO}_x$  and  $\text{NO}_y$ . Use of the parameterization based on the present dataset lies roughly between the two evaluations, with best agreement observed with NASA for the lower atmosphere. However, as previous laboratory studies had not identified the important role of  $\text{H}_2\text{O}$  in the title reaction, which could therefore not be incorporated in either of the previous parameterizations, any agreement at better than 10% level is fortuitous, reflecting random cancelling of systematic bias.

As reaction with OH is the predominant sink for most atmospheric trace-gases, its concentration largely defines the oxidizing power of the atmosphere (Lelieveld et al., 2004; Lelieveld et al., 2008; Lelieveld et al., 2016b) and even changes of a few percent in its concentration are significant. An increase in the rate coefficient of the title reaction will reduce the atmospheric abundance of this centrally important radical. In Fig. S10 we illustrate the impact of using the parameterization of  $k_1$  from the present study compared to the IUPAC and NASA recommendations. The upper panel in Fig. S10 plots the ratio of OH concentrations obtained when using the IUPAC parameterization and that from the present study,  $\text{OH(IUPAC)} / \text{OH(this work)}$ . Throughout the troposphere  $\text{OH(IUPAC)} / \text{OH(this work)}$  deviates by only a few percent, with a value of 1.02 at the surface and 0.96 at the tropical tropopause.  $\text{OH(NASA)} / \text{OH(this work)}$  is also 1.02 at the surface but increases to 1.04 at the tropical tropopause as the NASA-derived value of  $k_1$  is lower at the temperatures and pressures encountered in this part of the atmosphere. The weak effect of changing  $k_1$  on OH at the surface reflects the fact that many reactions apart from that with  $\text{NO}_2$  contribute to the overall sink term for OH in the lower troposphere.

Although our experiments do not give insight into the branching between formation of  $\text{HOONO}$  and  $\text{HNO}_3$  in the title reaction, previous work predicts a significant yield of  $\text{HOONO}$  especially at low temperatures (see Fig S8). As the lifetime of  $\text{HOONO}$  with respect to re-dissociation to reactants is short at e.g. boundary layer temperatures ( $\approx 1$  s at 298 K and 1 bar pressure), its formation may be seen as an effective reduction in the rate coefficient for  $\text{OH} + \text{NO}_2$  (Golden and Smith, 2000). However, its lifetime increases to several days at temperature and pressure conditions typical e.g. of the tropical tropopause (100 mbar, 220 K). As  $\text{HOONO}$  formation and loss are now parameterized (see above) in EMAC, we can explore its potential contribution to odd-nitrogen species in the atmosphere. The reaction between OH and  $\text{NO}_2$  to form  $\text{HOONO}$  converts short lived  $\text{HO}_x$  ( $\text{HO}_x = \text{OH} + \text{HO}_2$ ) and  $\text{NO}_x$  ( $\text{NO}_x = \text{NO} + \text{NO}_2$ ) into a longer lived “reservoir” species, and in this sense is similar to the reaction between  $\text{HO}_2$  and  $\text{NO}_2$  to form  $\text{HO}_2\text{NO}_2$



which is also thermally unstable, dissociating to reform  $\text{HO}_2$  and  $\text{NO}_2$ . Unlike  $\text{HOONO}$ , for which there are no atmospheric measurements, much effort has been made to measure concentrations of  $\text{HO}_2\text{NO}_2$  in colder regions of the atmosphere and it is considered an important component of the  $\text{NO}_y$  budget at high altitudes (Nault et al., 2016). We therefore compared EMAC predictions of  $\text{HOONO}$  concentrations with those of  $\text{HO}_2\text{NO}_2$ . The results are displayed in Fig. 8, in which we plot the zonally averaged  $\text{HOONO} / \text{HO}_2\text{NO}_2$  ratio. Immediately apparent from Fig. 8 is that, compared to  $\text{HO}_2\text{NO}_2$ ,  $\text{HOONO}$  is a minor component of  $\text{NO}_y$  in the warm, lower atmosphere. This reflects the difference in the thermal decomposition rate constant of the two trace gases, that of  $\text{HO}_2\text{NO}_2$  being  $\approx 4 \times 10^{-5} \text{ s}^{-1}$  in e.g. the middle troposphere at 400 mbar and 250 K, whereas  $\text{HOONO}$  decomposes a factor 30 faster so that its lifetime is only  $\approx 1000$  s. In the UTLS region, the ratio increases further ( $\text{HO}_2\text{NO}_2$  is a factor 50 more long-lived w.r.t. thermal decomposition at 100 mbar and 220 K) but the lifetimes of both gases under these conditions are sufficiently long that their concentrations are largely determined by their production rates and their losses due to photolysis and reaction with OH. The maximum ratio of  $\text{HOONO}$  to  $\text{HO}_2\text{NO}_2$  is found at the tropical tropopause, where concentrations become comparable. As the modelled loss processes of  $\text{HOONO}$  and  $\text{HO}_2\text{NO}_2$  (rate constants for photolysis and reaction with OH) are assumed to be identical, the occurrence of the maximum  $\text{HOONO}$  to  $\text{HO}_2\text{NO}_2$  ratio at the tropical tropopause is related to the ratio of the (temperature dependent) rate coefficients responsible for their formation (at 220 K and 100 mbar this favours  $\text{HOONO}$  formation by a factor of  $\approx 2$ ) and the model  $\text{OH} / \text{HO}_2$  ratio. Whilst this result

indicates that HOONO could be an important reservoir of NO<sub>x</sub> under certain conditions, we must bear in mind that there is great uncertainty associated not only with the branching ratio to HOONO formation in R1b but also with its loss processes (reaction with OH, photolysis), which remain unexplored experimentally. OH reacts with HO<sub>2</sub>NO<sub>2</sub> via H-abstraction from the H-OO group (IUPAC, 2019), and a similar mechanism is likely for HOONO. As the H-OO bond strength is likely to be greater in HOONO than in HO<sub>2</sub>NO<sub>2</sub> (larger electron density around the peroxy bond) we may expect the rate coefficient to be lower for HOONO. A significantly lower rate coefficient for reaction with OH (or photolysis rate constant) could greatly increase the abundance of HOONO. If this were the case, airborne instruments that measure NO<sub>x</sub> would likely also measure some fraction of HOONO following its rapid decomposition in warm inlet lines, as has been observed for HO<sub>2</sub>NO<sub>2</sub> and CH<sub>3</sub>O<sub>2</sub>NO<sub>2</sub> (Nault et al., 2015; Silvern et al., 2018). Clearly, more experimental or theoretical data that better constrain the yield of HOONO and its atmospheric loss processes as well as atmospheric measurements are necessary in order to improve our understanding of the role of the reaction between OH and NO<sub>2</sub> throughout the atmosphere.

#### 4 Conclusions

We have made very precise and accurate measurements for the overall rate coefficient,  $k_1$ , of the reaction between OH and NO<sub>2</sub>, which is of critical importance in atmospheric chemistry. Our experiments demonstrate clearly that the presence of H<sub>2</sub>O increases significantly the overall rate coefficient ( $k_1$ ) of the reaction between OH and NO<sub>2</sub>. H<sub>2</sub>O is found to be a more efficient collisional quencher (by a factor of  $\approx 6$ ) of the initially formed HO-NO<sub>2</sub> association complex than N<sub>2</sub> and a factor  $\approx 8$  more efficient than O<sub>2</sub>. A new parameterisation of the rate coefficient for the title reaction that considers the roles of N<sub>2</sub>, O<sub>2</sub> and H<sub>2</sub>O as third-body quenchers (also using data from our companion paper, Amedro et al. (2019)) has been incorporated into a global chemistry transport model to assess its impact on e.g. the HNO<sub>3</sub> / NO<sub>2</sub> ratio as well as NO<sub>x</sub> and OH levels. Compared to existing evaluations of the kinetic data, use of the new parameters will result in significant changes (5-10%) in the partitioning of NO<sub>x</sub> and NO<sub>y</sub>, the direction of the bias depending on which evaluation is used as reference and on region of the atmosphere. This work highlights the continuing importance of obtaining accurate laboratory kinetic data for those reactions that are central to our understanding of atmospheric chemistry and which provide anchor-points in chemical transport models. Though the result is associated with great uncertainty owing to missing kinetic parameters for HOONO, the global model predicts the presence of HOONO in concentrations similar to those of HO<sub>2</sub>NO<sub>2</sub> at the tropical tropopause. The present dataset addresses only the overall rate coefficient,  $k_1$ . Detailed experimental studies of the formation of HOONO (e.g. its yield at various temperatures and in the presence of H<sub>2</sub>O) and on the fate of HOONO (OH kinetics, photolysis) are required to better assess its role as NO<sub>x</sub> and HO<sub>x</sub> reservoir in cold parts of the atmosphere.

*Data availability.* The rate coefficients measured during this experimental study are listed in Table 1.

*Author contributions.* The experiments were carried out by DA, AJCB, and MB. The data analysis and preparation of the paper were performed by DA, with assistance from JL and JNC. The global modelling was performed by AP.

*Competing interests.* The authors declare that they have no conflict of interest.

*Financial support.* The article processing charges for this open access publication were covered by the Max Planck Society.

## References

- Allodi, M. A., Dunn, M. E., Livada, J., Kirschner, K. N., and Shields, G. C.: Do hydroxyl radical-water clusters,  $\text{OH}(\text{H}_2\text{O})(n)$ ,  $n=1-5$ , exist in the atmosphere?, *J. Phys. Chem. A*, 110, 13283-13289, doi:10.1021/jp064468l, 2006.
- Amedro, D., Bunkan, A. J. C., Berasategui, M., and Crowley, J. N.: Kinetics of the  $\text{OH} + \text{NO}_2$  reaction: rate coefficients (217–333 K, 16–1200mbar) and fall-off parameters for  $\text{N}_2$  and  $\text{O}_2$  bath gases, *Atmos. Chem. Phys.*, 19, 10643-10657, doi:10.5194/acp-19-10643-2019, 2019.
- Anastasi, C., and Smith, I. W. M.: Rate measurements of reactions of OH by resonance absorption. Part 5.-Rate constants for  $\text{OH} + \text{NO}_2 (+\text{M}) \rightarrow \text{HNO}_3 (+\text{M})$  over a wide range of temperature and pressure, *Journal of the Chemical Society, Faraday Transactions 2: Molecular and Chemical Physics*, 72, 1459-1468, doi:10.1039/f29767201459, 1976.
- Anderson, J. G., Margitan, J. J., and Kaufman, F.: Gas-phase recombination of OH with NO and  $\text{NO}_2$ , *J. Chem. Phys.*, 60, 3310-3317, 1974.
- Anderson, L. G.: Absolute rate constants for the reaction of OH with  $\text{NO}_2$  in  $\text{N}_2$  and He from 225 to 389 K, *J. Phys. Chem.*, 84, 2152-2155, 1980.
- Burke, M. P., and Song, R.: Evaluating mixture rules for multi-component pressure dependence:  $\text{H} + \text{O}_2 (+\text{M}) = \text{HO}_2 (+\text{M})$ , *Proceedings of the Combustion Institute*, 36, 245-253, doi:<https://doi.org/10.1016/j.proci.2016.06.068>, 2017.
- Burkholder, J. B., Sander, S. P., Abbatt, J., Barker, J. R., Huie, R. E., Kolb, C. E., Kurylo, M. J., Orkin, V. L., Wilmouth, D. M., and Wine, P. H.: Chemical Kinetics and Photochemical Data for Use in Atmospheric Studies, Evaluation No. 18," JPL Publication 15-10, Jet Propulsion Laboratory, Pasadena, <http://jpldataeval.jpl.nasa.gov>, 2015.
- Buszek, R. J., Francisco, J. S., and Anglada, J. M.: Water effects on atmospheric reactions, *International Reviews in Physical Chemistry*, 30, 335-369, doi:10.1080/0144235X.2011.634128, 2011.
- Cantrell, C. A., Zimmer, A., and Tyndall, G. S.: Absorption cross sections for water vapor from 183 to 193 nm, *Geophys. Res. Lett.*, 24, 2195-2198, 1997.
- Cobos, C. J., and Troe, J.: Prediction of reduced falloff curves for recombination reactions at low temperatures, *Z. Phys. Chem.*, 217, 1031-1044, 2003.
- D'Ottone, L., Campuzano-Jost, P., Bauer, D., and Hynes, A. J.: A pulsed laser photolysis-pulsed laser induced fluorescence study of the kinetics of the gas-phase reaction of OH with  $\text{NO}_2$ , *J. Phys. Chem. A*, 105, 10538-10543, 2001.
- D'Ottone, L., Bauer, D., Campuzano-Jost, P., Fardy, M., and Hynes, A. J.: Kinetic and mechanistic studies of the recombination of OH with  $\text{NO}_2$ : Vibrational deactivation, isotopic scrambling and product isomer branching ratios, *Faraday Discussions*, 130, 111-123, 2005.
- de Meij, A., Pozzer, A., Pringle, K. J., Tost, H., and Lelieveld, J.: EMAC model evaluation and analysis of atmospheric aerosol properties and distribution with a focus on the Mediterranean region, *Atmospheric Research*, 114, 38-69, 2012.
- Deckert, R., Jockel, P., Grewe, V., Gottschaldt, K. D., and Hoor, P.: A quasi chemistry-transport model mode for EMAC, *Geoscientific Model Development*, 4, 195-206, 2011.
- Dulitz, K., Amedro, D., Dillon, T. J., Pozzer, A., and Crowley, J. N.: Temperature-(208-318 K) and pressure-(18-696 Torr) dependent rate coefficients for the reaction between OH and  $\text{HNO}_3$ , *Atmos. Chem. Phys.*, 18, 2381-2394, 2018.
- Elshorbany, Y. F., Crutzen, P. J., Steil, B., Pozzer, A., Tost, H., and Lelieveld, J.: Global and regional impacts of HONO on the chemical composition of clouds and aerosols, *Atmos. Chem. Phys.*, 14, 1167-1184, 2014.
- Erler, K., Field, D., Zellner, R., and Smith, I. W. M.: Recombination reaction between hydroxyl radicals and nitrogen-dioxide:  $\text{OH} + \text{NO}_2 + \text{M} (= \text{He}, \text{CO}_2)$  in temperature range 213-300K, *Berichte Der Bunsen-Gesellschaft-Physical Chemistry Chemical Physics*, 81, 22-26, doi:10.1002/bbpc.19770810107, 1977.
- Fernandes, R. X., Luther, K., Troe, J., and Ushakov, V. G.: Experimental and modelling study of the recombination reaction  $\text{H} + \text{O}_2 (+\text{M}) \rightarrow \text{HO}_2 (+\text{M})$  between 300 and 900 K, 1.5 and 950 bar, and in the bath gases  $\text{M} = \text{He}, \text{Ar}$ , and  $\text{N}_2$ , *Phys. Chem. Chem. Phys.*, 10, 4313-4321, doi:10.1039/b804553d, 2008.
- Getzinger, R. W., and Blair, L. S.: Recombination in the hydrogen-oxygen reaction: A shock tube study with nitrogen and water vapour as third bodies, *Combust. Flame*, 13, 271-284, doi:[https://doi.org/10.1016/0010-2180\(69\)90005-4](https://doi.org/10.1016/0010-2180(69)90005-4), 1969.
- Gilbert, R. G., Luther, K., and Troe, J.: Theory of thermal unimolecular reactions in the fall-off range .2. weak collision rate constants, *Berichte Der Bunsen-Gesellschaft-Physical Chemistry Chemical Physics*, 87, 169-177, 1983.
- Glänzer, K., and Troe, J.: Thermal Decomposition of Nitrocompounds in Shock Waves. IV: Decomposition of Nitric Acid, *Berichte der Bunsengesellschaft für physikalische Chemie*, 78, 71-76, doi:10.1002/bbpc.19740780112, 1974.
- Golden, D. M., and Smith, G. P.: Reaction of  $\text{OH} + \text{NO}_2 + \text{M}$ : A new view, *J. Phys. Chem. A*, 104, 3991-3997, 2000.
- Golden, D. M., Barker, J. R., and Lohr, L. L.: Master equation models for the pressure- and temperature-dependant reactions  $\text{HO} + \text{NO}_2 \rightarrow \text{HONO}_2$  and  $\text{HO} + \text{NO}_2 \rightarrow \text{HOONO}$ , *J. Phys. Chem. A*, 107, 11057-11071, 2003.
- Hippler, H., Krasteva, N., Nasterlack, S., and Striebel, F.: Reaction of OH +  $\text{NO}_2$ : High pressure experiments and falloff analysis, *J. Phys. Chem. A*, 110, 6781-6788, 2006.
- IUPAC: Task Group on Atmospheric Chemical Kinetic Data Evaluation, (Ammann, M., Cox, R.A., Crowley, J.N., Herrmann, H., Jenkin, M.E., McNeill, V.F., Mellouki, A., Rossi, M. J., Troe, J. and Wallington, T. J.) <http://iupac.pole-ether.fr/index.html>, 2019.
- Jeuken, A. B. M., Siegmund, P. C., Heijboer, L. C., Feichter, J., and Bengtsson, L.: On the potential of assimilating meteorological analyses in a global climate model for the purpose of model validation, *J. Geophys. Res. -Atmos.*, 101, 16939-16950, 1996.
- Jöckel, P., Tost, H., Pozzer, A., Bruhl, C., Buchholz, J., Ganzeveld, L., Hoor, P., Kerkweg, A., Lawrence, M. G., Sander, R., Steil, B., Stiller, G., Tanarhte, M., Taraborrelli, D., Van Aardenne, J., and Lelieveld, J.: The atmospheric chemistry general circulation model ECHAM5/MESSy1: consistent simulation of ozone from the surface to the mesosphere, *Atmos. Chem. Phys.*, 6, 5067-5104, 2006.
- Jöckel, P., Kerkweg, A., Pozzer, A., Sander, R., Tost, H., Riede, H., Baumgaertner, A., Gromov, S., and Kern, B.: Development cycle 2 of the Modular Earth Submodel System (MESSy2), *Geoscientific Model Development*, 3, 717-752, 2010.
- Kircher, C. C., and Sander, S. P.: Kinetics and mechanism of  $\text{HO}_2$  and  $\text{DO}_2$  disproportionations, *J. Phys. Chem.*, 88, 2082-2091, 1984.
- Lelieveld, J., Dentener, F. J., Peters, W., and Krol, M. C.: On the role of hydroxyl radicals in the self-cleansing capacity of the troposphere, *Atmos. Chem. Phys.*, 4, 2337-2344, 2004.
- Lelieveld, J., Butler, T. M., Crowley, J. N., Dillon, T. J., Fischer, H., Ganzeveld, L., Harder, H., Lawrence, M. G., Martinez, M., Taraborrelli, D., and Williams, J.: Atmospheric oxidation capacity sustained by a tropical forest, *Nature*, 452, 737-740, 2008.
- Lelieveld, J., Gromov, S., Pozzer, A., and Taraborrelli, D.: Global tropospheric hydroxyl distribution, budget and reactivity, *Atmos. Chem. Phys.*, 16, 12477-12493, 2016a.
- Lelieveld, J., Gromov, S., Pozzer, A., and Taraborrelli, D.: Global tropospheric hydroxyl distribution, budget and reactivity, *Atmos. Chem. Phys. Discuss.*, 2016, 1-25, doi:10.5194/acp-2016-160, 2016b.

- Lii, R.-R., Sauer, M. C., and Gordon, S.: Temperature dependence of the gas-phase self-reaction of HO<sub>2</sub> in the presence of H<sub>2</sub>O, *J. Phys. Chem.*, 85, 2833-2834, 1981.
- Michael, J. V., Su, M. C., Sutherland, J. W., Carroll, J. J., and Wagner, A. F.: Rate constants for H+O<sub>2</sub>+M → HO<sub>2</sub>+M in seven bath gases, *J. Phys. Chem. A*, 106, 5297-5313, doi:10.1021/jp020229w, 2002.
- Mollner, A. K., Valluvadasan, S., Feng, L., Sprague, M. K., Okumura, M., Milligan, D. B., Bloss, W. J., Sander, S. P., Martien, P. T., Harley, R. A., McCoy, A. B., and Carter, W. P. L.: Rate of gas phase association of hydroxyl radical and nitrogen dioxide, *Science*, 330, 646-649, doi:10.1126/science.1193030, 2010.
- Morley, C., and Smith, I. W. M.: Rate measurements of reactions of OH by resonance absorption. 1. Reactions of OH with NO<sub>2</sub> and NO, *Journal of the Chemical Society-Faraday Transactions II*, 68, 1016-&, doi:10.1039/f29726801016, 1972.
- Nault, B. A., Garland, C., Pusede, S. E., Wooldridge, P. J., Ullmann, K., Hall, S. R., and Cohen, R. C.: Measurements of CH<sub>3</sub>O<sub>2</sub>NO<sub>2</sub> in the upper troposphere, *Atmos. Meas. Tech.*, 8, 987-997, doi:10.5194/amt-8-987-2015, 2015.
- Nault, B. A., Garland, C., Wooldridge, P. J., Brune, W. H., Campuzano-Jost, P., Crounse, J. D., Day, D. A., Dibb, J., Hall, S. R., Huey, L. G., Jimenez, J. L., Liu, X. X., Mao, J. Q., Mikoviny, T., Peischl, J., Pollack, I. B., Ren, X. R., Ryerson, T. B., Scheuer, E., Ullmann, K., Wennberg, P. O., Wisthaler, A., Zhang, L., and Cohen, R. C.: Observational Constraints on the Oxidation of NO<sub>x</sub> in the Upper Troposphere, *J. Phys. Chem. A*, 120, 1468-1478, doi:10.1021/acs.jpca.5b07824, 2016.
- Newsome, B., and Evans, M.: Impact of uncertainties in inorganic chemical rate constants on tropospheric composition and ozone radiative forcing, *Atmos. Chem. Phys.*, 17, 14333-14352, doi:10.5194/acp-17-14333-2017, 2017.
- Pozzer, A., Pollmann, J., Taraborrelli, D., Jockel, P., Helmig, D., Tans, P., Hueber, J., and Lelieveld, J.: Observed and simulated global distribution and budget of atmospheric C-2-C-5 alkanes, *Atmos. Chem. Phys.*, 10, 4403-4422, 2010.
- Roeckner, E., Brokopf, R., Esch, M., Giorgetta, M., Hagemann, S., Kornblueh, L., Manzini, E., Schlese, U., and Schulzweida, U.: Sensitivity of simulated climate to horizontal and vertical resolution in the ECHAM5 atmosphere model, *Journal of Climate*, 19, 3771-3791, 2006.
- Sadanaga, Y., Kondo, S., Hashimoto, K., and Kajii, Y.: Measurement of the rate coefficient for the OH+NO<sub>2</sub> reaction under the atmospheric pressure: Its humidity dependence, *Chem. Phys. Lett.*, 419, 474-478, 2006.
- Sander, R., Baumgaertner, A., Cabrera-Perez, D., Frank, F., Gromov, S., Grooss, J. U., Harder, H., Huijnen, V., Jockel, P., Karydis, V. A., Niemeyer, K. E., Pozzer, A., Hella, R. B., Schultz, M. G., Taraborrelli, D., and Tauer, S.: The community atmospheric chemistry box model CAABA/MECCA-4.0, *Geoscientific Model Development*, 12, 1365-1385, doi:10.5194/gmd-12-1365-2019, 2019.
- Shao, J., Choudhary, R., Susa, A., Davidson, D. F., and Hanson, R. K.: Shock tube study of the rate constants for H + O<sub>2</sub> + M → HO<sub>2</sub> + M (M = Ar, H<sub>2</sub>O, CO<sub>2</sub>, N<sub>2</sub>) at elevated pressures, *Proceedings of the Combustion Institute*, 37, 145-152, doi:<https://doi.org/10.1016/j.proci.2018.05.077>, 2019.
- Silvern, R. F., Jacob, D. J., Travis, K. R., Sherwen, T., Evans, M. J., Cohen, R. C., Laughner, J. L., Hall, S. R., Ullmann, K., Crounse, J. D., Wennberg, P. O., Peischl, J., and Pollack, I. B.: Observed NO/NO<sub>2</sub> ratios in the upper troposphere imply errors in NO-NO<sub>2</sub>-O<sub>3</sub> cycling kinetics or an unaccounted NO<sub>x</sub> reservoir, *Geophys. Res. Lett.*, 45, 4466-4474, doi:10.1029/2018gl077728, 2018.
- Simonaitis, R., and Heicklen, J.: The reaction of OH with NO<sub>2</sub> and the deactivation of O(<sup>1</sup>D) by CO, *Int. J. Chem. Kinet.*, IV, 529-540, 1972.
- Smith, I. W., and Williams, M. D.: Vibrational-relaxation of OH(v=1) and OD(v=1) By HNO<sub>3</sub>, DNO<sub>3</sub>, H<sub>2</sub>O, NO and NO<sub>2</sub>, *Journal of the Chemical Society, Faraday Transactions 2: Molecular and Chemical Physics*, 81, 1849-1860, 1985.
- Tao, F. M., Higgins, K., Klemperer, W., and Nelson, D. D.: Structure, binding energy, and equilibrium constant of the nitric acid-water complex, *Geophys. Res. Lett.*, 23, 1797-1800, 1996.
- Thomsen, D. L., Kurten, T., Jorgensen, S., Wallington, T. J., Baggesen, S. B., Aalling, C., and Kjaergaard, H. G.: On the possible catalysis by single water molecules of gas-phase hydrogen abstraction reactions by OH radicals, *Phys. Chem. Chem. Phys.*, 14, 12992-12999, doi:10.1039/c2cp40795g, 2012.
- Troe, J.: Mixture Rules in Thermal Unimolecular Reactions, *Berichte der Bunsengesellschaft für physikalische Chemie*, 84, 829-834, doi:10.1002/bbpc.19800840902, 1980.
- Troe, J.: Theory of thermal unimolecular reactions in the fall-off range 1. Strong collision rate constants, *Berichte Der Bunsen-Gesellschaft-Physical Chemistry Chemical Physics*, 87, 161-169, 1983.
- Troe, J.: Analysis of the temperature and pressure dependence of the reaction HO+NO<sub>2</sub>+M → HONO<sub>2</sub>+M, *Int. J. Chem. Kinet.*, 33, 878-889, 2001.
- Troe, J.: Toward a Quantitative Analysis of Association Reactions in the Atmosphere, *Chem. Rev.*, 103, 4565-4576, doi:10.1021/cr020514b, 2003.
- Troe, J., and Ushakov, V. G.: Revisiting falloff curves of thermal unimolecular reactions, *The Journal of Chemical Physics*, 135, 054304, doi:10.1063/1.3615542, 2011.
- Troe, J.: Refined representation of falloff curves for the reaction HO + NO<sub>2</sub> + N<sub>2</sub> → (HONO<sub>2</sub>, HOONO) + N<sub>2</sub>, *J. Phys. Chem. A*, 116, 6387-6393, doi:10.1021/jp212095n, 2012.
- Vandaele, A. C., Hermans, C., Fally, S., Carleer, M., Colin, R., Merienne, M. F., Jenouvrier, A., and Coquart, B.: High-resolution Fourier transform measurement of the NO<sub>2</sub> visible and near-infrared absorption cross sections: Temperature and pressure effects, *J. Geophys. Res.-Atmos.*, 107, Art. 4348, doi:10.1029/2001JD000971, 2002.
- Westenberg, A. A., and Dehaas, N.: Rate measurements on OH+NO+M and OH+NO<sub>2</sub>+M, *J. Chem. Phys.*, 57, 5375-+, doi:10.1063/1.1678234, 1972.
- Wine, P. H., Kreutter, N. M., and Ravishankara, A. R.: Flash photolysis-resonance fluorescence kinetics study of the reaction OH + NO<sub>2</sub> +M → HNO<sub>3</sub> + M, *J. Phys. Chem.*, 83, 3191-3195, 1979.
- Wollenhaupt, M., Carl, S. A., Horowitz, A., and Crowley, J. N.: Rate coefficients for reaction of OH with acetone between 202 and 395 K, *J. Phys. Chem.*, 104, 2695-2705, doi:10.1021/jp993738f, 2000.
- Yoon, J., and Pozzer, A.: Model-simulated trend of surface carbon monoxide for the 2001-2010 decade, *Atmos. Chem. Phys.*, 14, 10465-10482, 2014.

**Table 1. Measurements of  $k_1$  in He bath-gas**

$T$ (K)	$p$ (Torr)	$M^a$	OH precursor	$k_1^b$
277	48.6	1.68	H <sub>2</sub> O <sub>2</sub>	$1.59 \pm 0.14$
292	25.1	0.83	H <sub>2</sub> O <sub>2</sub> <sup>c</sup>	$0.75 \pm 0.07$
	50.0	1.65	H <sub>2</sub> O <sub>2</sub>	$1.37 \pm 0.08$
	75.1	2.47	H <sub>2</sub> O <sub>2</sub>	$1.88 \pm 0.12$
	102.9	3.39	HNO <sub>3</sub>	$2.32 \pm 0.15$
	206.9	6.81	HNO <sub>3</sub> <sup>d</sup>	$3.73 \pm 0.25$
	300.7	9.89	HNO <sub>3</sub>	$4.64 \pm 0.29$
	405.8	13.35	HNO <sub>3</sub>	$5.54 \pm 0.37$
	495.6	16.30	HNO <sub>3</sub>	$6.29 \pm 0.40$
	595.0	19.57	HNO <sub>3</sub>	$6.83 \pm 0.42$
	689.1	22.67	HNO <sub>3</sub>	$7.46 \pm 0.46$
	28.1	0.82	H <sub>2</sub> O <sub>2</sub>	$0.60 \pm 0.06$
332	56.8	1.65	H <sub>2</sub> O <sub>2</sub>	$0.99 \pm 0.08$
	85.4	2.48	H <sub>2</sub> O <sub>2</sub>	$1.34 \pm 0.10$

605

<sup>a</sup> Molecular density  $M(\text{He})$  in units of  $10^{18}$  molecule  $\text{cm}^{-3}$ . <sup>b</sup> Units of  $10^{-12}$   $\text{cm}^3$  molecule<sup>-1</sup> s<sup>-1</sup>. The errors are  $2\sigma$  total uncertainty.

<sup>c</sup>Concentration range of H<sub>2</sub>O<sub>2</sub>  $\approx 5\text{-}14 \times 10^{13}$  molecule  $\text{cm}^{-3}$ . <sup>d</sup>Concentration range of HNO<sub>3</sub>  $\approx 5\text{-}9 \times 10^{13}$  molecule  $\text{cm}^{-3}$ .



Table 2. Measurements of  $k_1$  in N<sub>2</sub>-H<sub>2</sub>O and He-H<sub>2</sub>O bath-gas

$T / \text{K}$	$p \text{ (Torr)}$	$M^a$	$[\text{H}_2\text{O}]^b$	$x_{\text{He}}$ or $x_{\text{N}_2}$	$x_{\text{H}_2\text{O}}$	$k_1^c$
N <sub>2</sub> -H <sub>2</sub> O bath gas						
292	50.2	1.65	0	1	0	$2.58 \pm 0.16$
	50.2	1.66	0.86	0.950	0.050	$3.07 \pm 0.22$
	50.0	1.65	1.62	0.905	0.095	$3.45 \pm 0.26$
	50.0	1.65	2.28	0.866	0.134	$3.83 \pm 0.26$
	50.2	1.66	2.84	0.834	0.166	$3.95 \pm 0.37$
	49.2	1.63	3.27	0.805	0.195	$4.10 \pm 0.27$
	50.0	1.65	4.06	0.754	0.246	$4.47 \pm 0.18^d$
He-H <sub>2</sub> O bath gas						
277	48.6	1.68	0	1	0	$1.59 \pm 0.11$
	47.6	1.66	0.9	0.946	0.054	$2.27 \pm 0.15$
	48.0	1.67	1.42	0.915	0.085	$2.63 \pm 0.17$
	48.7	1.7	2	0.882	0.118	$3.13 \pm 0.24$
291	50.0	1.65	0	1	0	$1.37 \pm 0.08$
	50.6	1.68	0.64	0.962	0.038	$1.99 \pm 0.14$
	51	1.69	1.30	0.923	0.077	$2.39 \pm 0.21$
	50.7	1.68	2.25	0.863	0.137	$2.88 \pm 0.24$
	49.5	1.64	3.06	0.818	0.182	$3.43 \pm 0.22$
	50.8	1.68	3.12	0.810	0.190	$3.44 \pm 0.24$
	49.7	1.65	3.60	0.783	0.217	$3.54 \pm 0.23$
	50.2	1.66	3.94	0.764	0.236	$3.72 \pm 0.29$
	50.5	1.67	4.68	0.721	0.279	$4.08 \pm 0.27$
332	56.8	1.65	0	1	0	$0.99 \pm 0.06$
	56.3	1.64	0.58	0.964	0.036	$1.32 \pm 0.08$
	56	1.63	1.72	0.895	0.105	$1.81 \pm 0.16$
	56.2	1.63	3.3	0.798	0.202	$2.43 \pm 0.18$
	55.9	1.62	4.33	0.733	0.267	$2.88 \pm 0.22$

Unless otherwise indicated, the measurements were performed using H<sub>2</sub>O<sub>2</sub> as OH precursor. The concentration range of H<sub>2</sub>O<sub>2</sub> was 5-18 × 10<sup>13</sup> molecule cm<sup>-3</sup> for experiments in He-H<sub>2</sub>O bath gas and 9-14 × 10<sup>13</sup> molecule cm<sup>-3</sup> for experiments in N<sub>2</sub>-H<sub>2</sub>O bath gas. <sup>a</sup> Molecular density M(He-H<sub>2</sub>O) or M(N<sub>2</sub>-H<sub>2</sub>O) in units of 10<sup>18</sup> molecule cm<sup>-3</sup>. <sup>b</sup> Units of 10<sup>17</sup> molecule cm<sup>-3</sup>. <sup>c</sup> Units of 10<sup>-12</sup> cm<sup>3</sup> molecule<sup>-1</sup> s<sup>-1</sup>. Errors are 2σ total uncertainty. <sup>d</sup> measurement performed using O<sub>3</sub>-H<sub>2</sub>O as OH precursor (with [O<sub>3</sub>] = 2 × 10<sup>13</sup> molecule cm<sup>-3</sup>).

**Table 3. Parameters for calculating  $k_1$  using Eqn. (15) and (16)**

Bath-gas	$k_0^a$	$T$ -dependence of $k_0$ ( $m$ , $q$ or $o$ )	$k_\infty^b$	$F_c$
N <sub>2</sub>	$2.6 \times 10^{-30}$	3.6 ( $m$ )	$6.3 \times 10^{-11}$	0.39
O <sub>2</sub>	$2.0 \times 10^{-30}$	3.6 ( $q$ )		
H <sub>2</sub> O	$15.9 \times 10^{-30}$	3.4 ( $o$ )		

620

<sup>a</sup> Units of cm<sup>6</sup> molecule<sup>-2</sup> s<sup>-1</sup>. <sup>b</sup> Units of cm<sup>3</sup> molecule<sup>-1</sup> s<sup>-1</sup>. Note that  $k_\infty$  is independent of temperature ( $n = 0$ ).



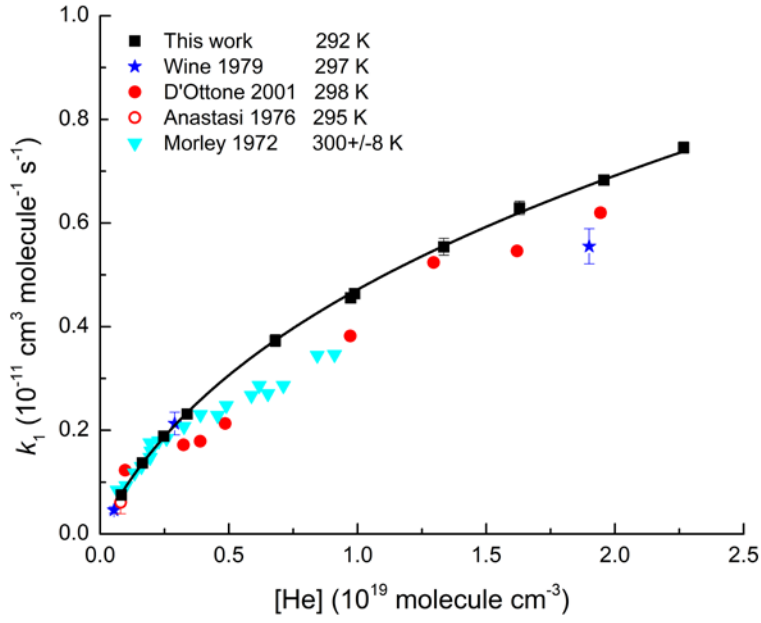


**Figure 1.** Values of  $k_1$  from this study (black squares) as a function of He concentration at 292 K. Errors are  $2\sigma$  statistical only. The solid line is a fit to our data using Eqn. (4) with  $k_0 = 1.4 \times 10^{-30} \text{ cm}^6 \text{ molecule}^{-2} \text{ s}^{-1}$ ,  $k_\infty = 6.3 \times 10^{-11} \text{ cm}^3 \text{ molecule}^{-1} \text{ s}^{-1}$ ,  $F_c = 0.32$ ,  $m = 3.1$  and  $n = 0$ . Previous datasets at room temperature (Wine et al. (1979), D'Ottone et al. (2001), Anastasi and Smith (1976) and Morley and Smith (1972)) are displayed for comparison.

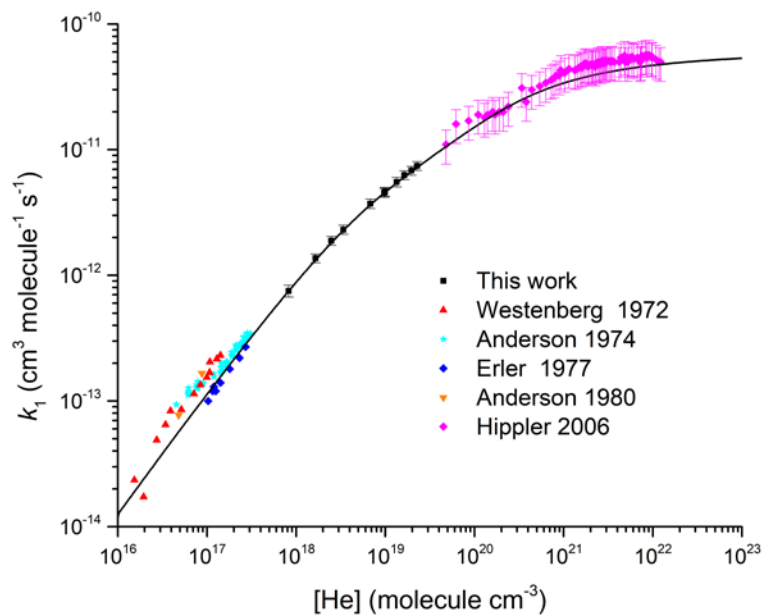


**Figure 2.** Comparison between the present dataset, the high pressure measurements by Hippler et al. (2006) and the low pressure measurements by Anderson et al. (1974), Westenberg and Dehaas (1972), Anderson (1980) and Erler et al. (1977). All measurements were made at room-temperature. The black line is our parameterisation with  $k_0 = 1.4 \times 10^{-30} \text{ cm}^6 \text{ molecule}^{-2} \text{ s}^{-1}$ ,  $k_\infty = 6.3 \times 10^{-11} \text{ cm}^3 \text{ molecule}^{-1} \text{ s}^{-1}$ ,  $m = 3.1$ ,  $n = 0$  and  $F_c = 0.32$ .

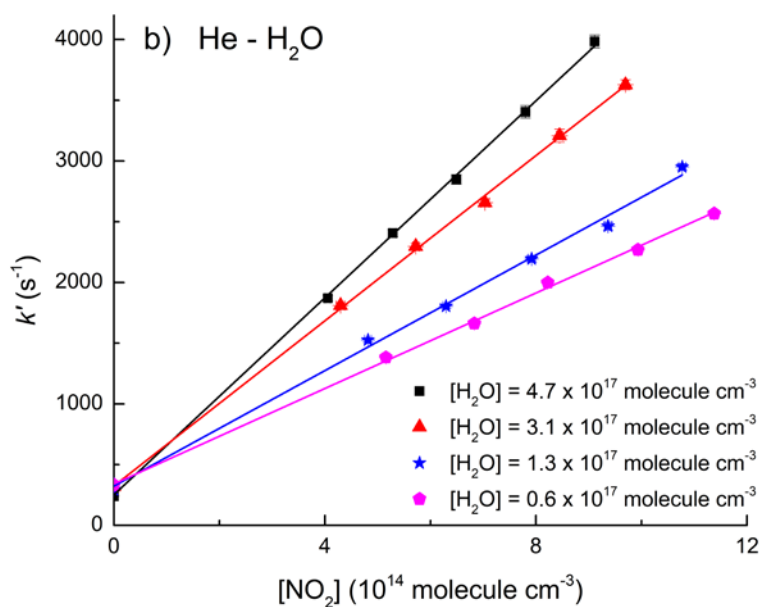
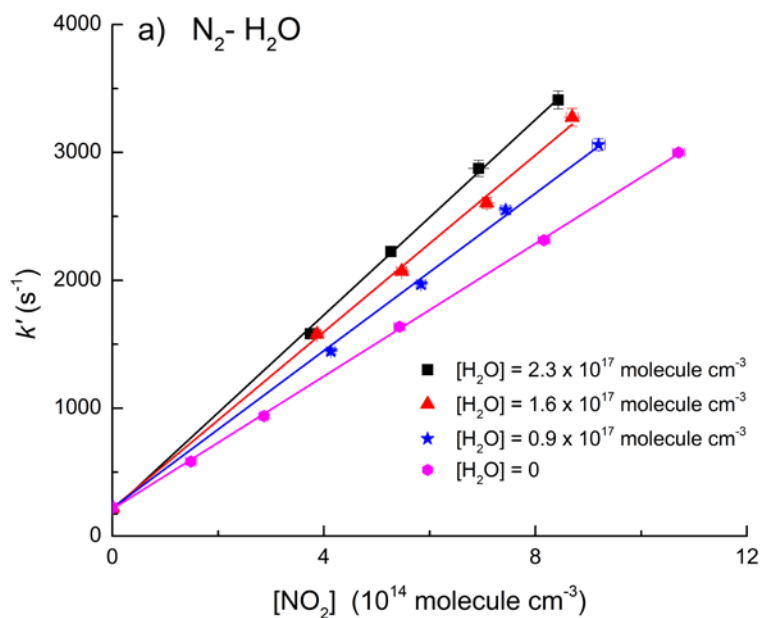


**Figure 3** a) Data obtained in  $\text{N}_2\text{-H}_2\text{O}$  bath-gas (50 Torr, 292 K). b) Data obtained in  $\text{He-H}_2\text{O}$  bath-gas (50 Torr, 291 K). Both panels display first-order, OH decay constants in various concentrations of  $\text{NO}_2$  and different mole fractions of  $\text{H}_2\text{O}$ . The solid lines represent least squares linear fits to Eqn. (2).

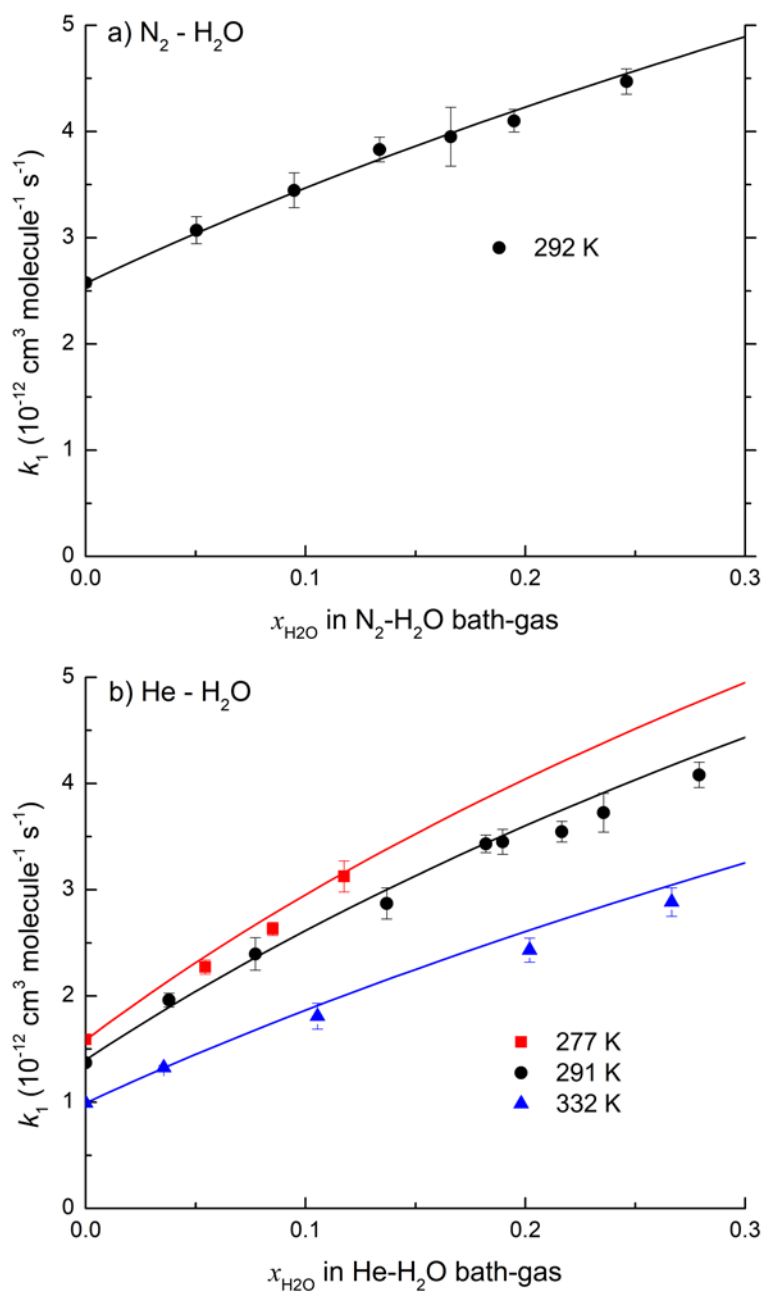


**Figure 4.** a)  $k_1$  as a function of  $x_{\text{H}_2\text{O}}$  at 50 Torr  $\text{N}_2\text{-H}_2\text{O}$  and 292 K. The line represents a least squares, multivariate fit (Eqn. 7 and 8) with  $k_\infty = 6.3 \times 10^{-11} \text{ cm}^3 \text{ molecule}^{-2} \text{ s}^{-1}$ ,  $k_0^{\text{N}_2} = 2.6 \times 10^{-30} \text{ cm}^6 \text{ molecule}^{-2} \text{ s}^{-1}$ ,  $F_c = 0.39$ ,  $m = 3.6$ ,  $k_0^{\text{H}_2\text{O}} = 15.9 \times 10^{-30} \text{ cm}^6 \text{ molecule}^{-2} \text{ s}^{-1}$ ,  $o = 3.4$ . b)  $k_1$  as a function of  $x_{\text{H}_2\text{O}}$  in  $\text{He-H}_2\text{O}$  mixtures at 277, 291 and 332 K. The solid lines represent a least squares, multivariate fit (Eqn. 7 and 9 to 12) where  $k_\infty = 6.3 \times 10^{-11} \text{ cm}^3 \text{ molecule}^{-2} \text{ s}^{-1}$ ,  $k_0^{\text{He}} = 1.4 \times 10^{-30} \text{ cm}^6 \text{ molecule}^{-2} \text{ s}^{-1}$ ,  $F_c^{\text{He}} = 0.32$ ,  $m = 3.1$ ,  $k_0^{\text{H}_2\text{O}} = 15.9 \times 10^{-30} \text{ cm}^6 \text{ molecule}^{-2} \text{ s}^{-1}$ ,  $F_c^{\text{H}_2\text{O}} = 0.39$  and  $o = 3.4$ .

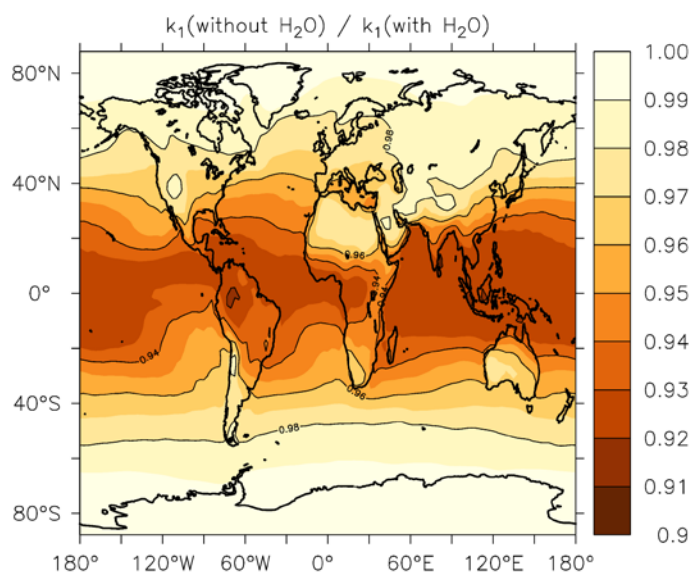


**Figure 5.** Annual average effect of H<sub>2</sub>O on  $k_1$  expressed as the fractional change in the rate coefficient at the Earth's surface when setting the mole fraction of water vapour to zero in Eqn. 15.

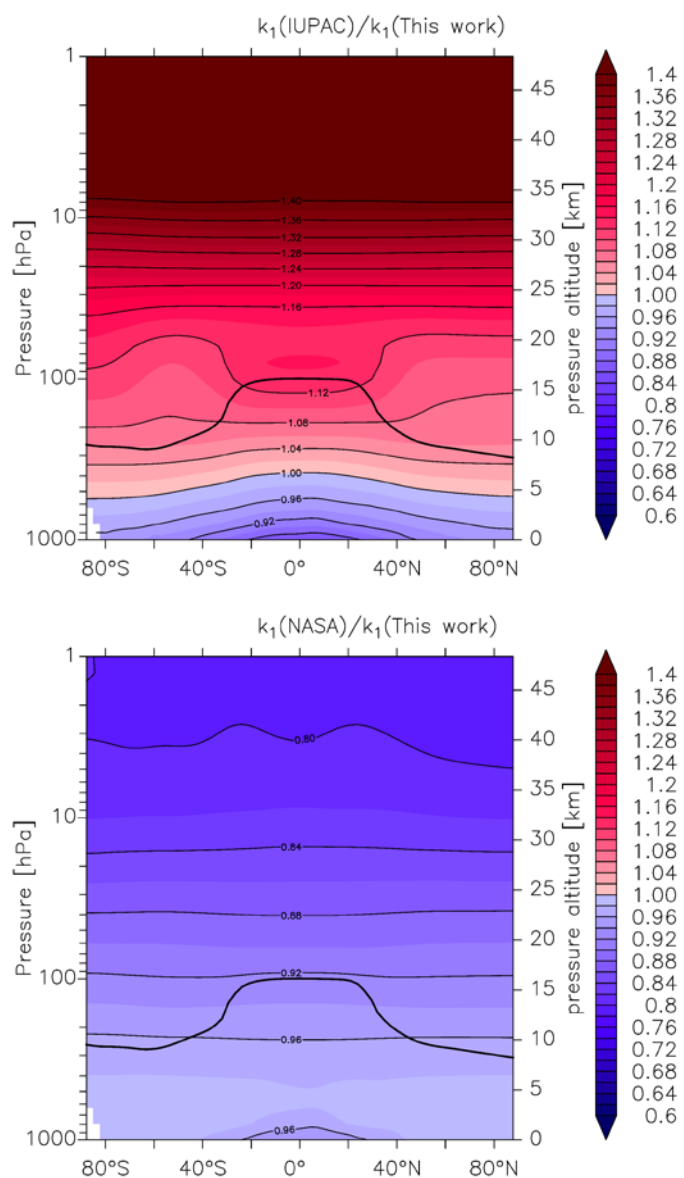


**Fig. 6** Global values of  $\frac{k_1^{\text{IUPAC}}}{k_1^{\text{this work}}}$  (upper panel) and  $\frac{k_1^{\text{NASA}}}{k_1^{\text{this work}}}$  (lower panel).  $k_1$  is the overall rate coefficient (both channels) for Reaction R1 calculated using the parameters from this work ( $k_1^{\text{this work}}$ ) and those presently recommended by the IUPAC ( $k_1^{\text{IUPAC}}$ ) and NASA ( $k_1^{\text{NASA}}$ ) data evaluation panels. The black line represents the model tropopause.

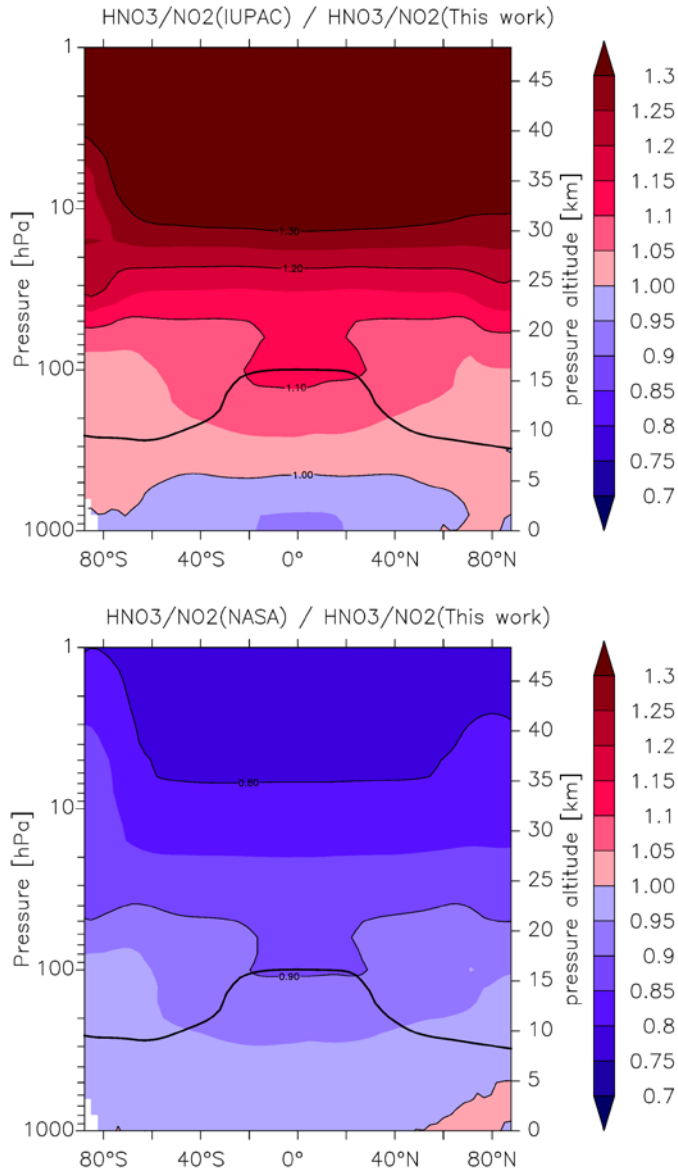


**Figure 7.** Effect of different parameterisations of  $k_1$  on the global (zonal and yearly averaged)  $\text{HNO}_3$  to  $\text{NO}_2$  ratio. The upper panel plots  $\frac{\text{HNO}_3}{\text{NO}_2}(\text{IUPAC}) / \frac{\text{HNO}_3}{\text{NO}_2}(\text{this work})$ , the lower panel plots  $\frac{\text{HNO}_3}{\text{NO}_2}(\text{NASA}) / \frac{\text{HNO}_3}{\text{NO}_2}(\text{this work})$ . The black line represents the model tropopause.

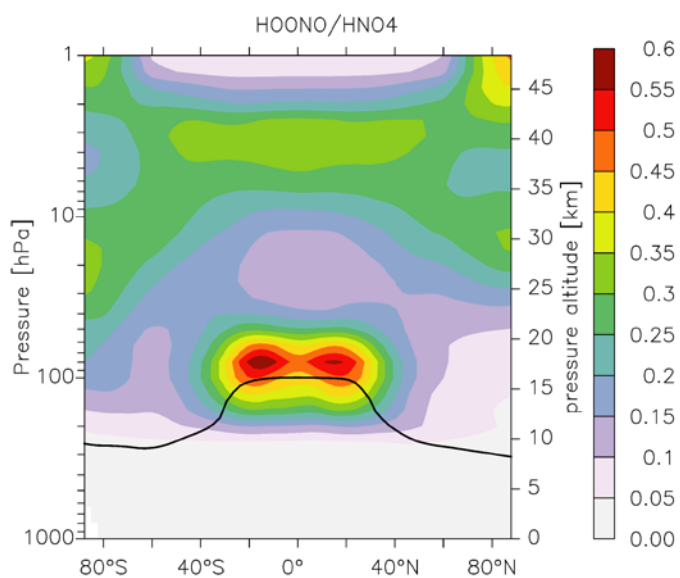


**Figure 8.** Model (EMAC) ratio of HOONO (formed in the reaction of  $\text{NO}_2$  with OH) to  $\text{HO}_2\text{NO}_2$  (formed in the reaction of  $\text{NO}_2$  with  $\text{HO}_2$ ) calculated using the present parameterisation of  $k_1$  and equating the (unknown) rate coefficients for loss of HOONO via reaction with OH or photolysis to those of  $\text{HO}_2\text{NO}_2$ . The black line represents the model tropopause.